ORIGINAL RESEARCH

Pharmacological Inhibitor of Notch Signaling Stabilizes the Progression of Small Abdominal Aortic Aneurysm in a Mouse Model

Jeeyun Cheng, BS;* Sara N. Koenig, BA;* Helena S. Kuivaniemi, MD, PhD; Vidu Garg, MD; Chetan P. Hans, PhD

***Background*—**The progression of abdominal aortic aneurysm (AAA) involves a sustained influx of proinflammatory macrophages, which exacerbate tissue injury by releasing cytokines, chemokines, and matrix metalloproteinases. Previously, we showed that Notch deficiency reduces the development of AAA in the angiotensin II–induced mouse model by preventing infiltration of macrophages. Here, we examined whether Notch inhibition in this mouse model prevents progression of small AAA and whether these effects are associated with altered macrophage differentiation.

***Methods and Results*—**Treatment with pharmacological Notch inhibitor (DAPT [N-(N-[3,5-difluorophenacetyl]-L-alanyl)-S-phenylglycine t-butyl ester]) at day 3 or 8 of angiotensin II infusion arrested the progression of AAA in *Apoe*$^{-/-}$ mice, as demonstrated by a decreased luminal diameter and aortic width. The abdominal aortas of *Apoe*$^{-/-}$ mice treated with DAPT showed decreased expression of matrix metalloproteinases and presence of elastin precursors including tropoelastin and hyaluronic acid. Marginal adventitial thickening observed in the aorta of DAPT-treated *Apoe*$^{-/-}$ mice was not associated with increased macrophage content, as observed in the mice treated with angiotensin II alone. Instead, DAPT-treated abdominal aortas showed increased expression of Cd206-positive M2 macrophages and decreased expression of Il12-positive M1 macrophages. Notch1 deficiency promoted M2 differentiation of macrophages by upregulating transforming growth factor β2 in bone marrow–derived macrophages at basal levels and in response to IL4. Protein expression of transforming growth factor β2 and its downstream effector pSmad2 also increased in DAPT-treated *Apoe*$^{-/-}$ mice, indicating a potential link between Notch and transforming growth factor β2 signaling in the M2 differentiation of macrophages.

***Conclusions*—**Pharmacological inhibitor of Notch signaling prevents the progression of AAA by macrophage differentiation–dependent mechanisms. The study also provides insights for novel therapeutic strategies to prevent the progression of small AAA.
(*J Am Heart Assoc*. 2014;3:e001064 doi: 10.1161/JAHA.114.001064)

Key Words: abdominal aortic aneurysm • macrophage differentiation • Notch1 • Tgfβ2

Abdominal aortic aneurysm (AAA) is a localized dilation of the abdominal aorta exceeding the normal diameter by more than 50% of its original size.[1,2] The prevalence of AAA ranges from 1.3% in men aged 45 to 54 years to ≈10% in those older than 65 years.[1,3] Although advancements in diagnostic methods and watchful monitoring have been effective in reducing the risk of rupture, aortic aneurysms still account for more than 10 000 deaths each year in the United States alone.[1] The only treatment options for AAA are surgical or catheter-based interventions and are indicated after the aneurysm exceeds a threshold size. However, surgical interventions carry certain risks, come with an associated financial burden, and do not provide long-term survival advantage for the repair of small AAA.[4] Only with an increased understanding of the mechanisms underlying the progression of AAA will novel, nonsurgical, cost-effective therapies be devised to reduce AAA progression and rupture.[5–7]

Aneurysm research using mouse models and diseased human tissues over the past 2 decades has identified the presence of mononuclear inflammatory cell infiltrate and augmented proteolytic activity as key features of AAA.[8–10] Although multiple pathogenic pathways converge to promote AAA progression,[11] the critical stimulus seems to be the differentiation of naïve monocyte macrophages into the

From the Center for Cardiovascular and Pulmonary Research and The Heart Center, Nationwide Children's Hospital (J.C., S.N.K., V.G., C.P.H.) and Departments of Pediatrics (V.G., C.P.H.) and Molecular Genetics (V.G.), The Ohio State University, Columbus, OH; The Sigfried and Janet Weis Center for Research, Geisinger Health System, Danville, PA (H.S.K.).

*Dr Cheng and Dr Koenig contributed equally to the manuscript.

Correspondence to: Chetan P. Hans, PhD, Heart Center and Center of Cardiovascular and Pulmonary Research, Research Building III, Room WB4235, Nationwide Children's Hospital, 575 Children's Crossroads Columbus, OH 43205. E-mail: chetan.hans@nationwidechildrens.org

Received January 7, 2014; accepted June 19, 2014.

highly infiltrative M1 phenotype in response to aortic injury.[12] The sustained influx of proinflammatory M1 macrophages releases matrix metalloproteinases (MMPs) and cytokines leading to the depletion of medial smooth muscle cells.[13] Activation of MMPs also results in dissolution of the elastin and interstitial collagenous matrix of the medial layer of aorta.[8] Alternatively, macrophages also have the ability to program into the M2-phenotype, which inhibit the inflammatory response and promotes tissue repair by mechanisms dependent on transforming growth factor β2 (Tgfβ2).[14] Despite major advances in our understanding of the various functions of macrophages in AAA, little is known about the regulation of macrophage differentiation and their role in AAA pathogenesis.

Notch signaling is involved in multiple aspects of vascular development, smooth muscle cell proliferation, myeloid differentiation, and inflammation.[15–17] The Notch signaling pathway consists of a family of 4 Notch receptors (1 to 4) that interact with the Jagged and Delta ligand families. In the canonical signaling pathway, Notch1 is activated following receptor-ligand binding at the cell surface that induces proteolytic cleavage by several proteases, including γ-secretase.[18] This cleavage results in the release and translocation of the Notch1 intracellular domain (NICD) into the nucleus, where it interacts with the transcription factor CBF-1 (also known as RBP-J or CSL) to promote transcriptional activation of downstream effectors.[18–20] Although Notch1 is essential for embryonic survival,[21] increased expression of Notch1 is reported in thoracic aortic aneurysms and dissections,[21] AAA,[22–23] atherosclerosis,[24] and a variety of cancers[25] and is highly associated with inflammatory macrophages.[15] Specifically, Notch1 has been suggested to regulate the expression of key inflammatory genes including *Mcp1*, inducible nitric oxide synthase (*iNOS*), *Icam1*, and *Vcam1* in macrophages.[15,22,26] The proinflammatory effects of Notch1 signaling have been linked to modulation of macrophage functions, including differentiation and infiltration at the vascular injury site.[27–29] Recent publications have suggested that the Notch–RBP-J pathway controls the expression of prototypical M1 effector molecules, such as Il12 and iNOS, suggesting its role in the M1 polarization of macrophages.[22,29,30] However, its exact roles in M2 differentiation and functional consequences of such regulation in AAA are obscure.

Our previous studies have demonstrated that *Notch1* haploinsufficiency or pharmacologic inhibition prior to the development of aneurysmal dilation at days −7 and +3 of angiotensin II (AngII) infusion dramatically reduces the development of AAA in mice by preventing infiltration of macrophages at the site of vascular injury. This is associated with decreased expression of cytokines and chemokines.[22] Recent studies have substantiated our data on the protective roles for Notch1 deficiency in the development of AAA; however, its role in the progression of AAA is still speculative.[21,23] In this study, we sought to determine the effect of pharmacological inhibition of Notch signaling (DAPT [N-(N-[3,5-difluorophenacetyl]-L-alanyl)-S-phenylglycine t-butyl ester]) on the progression of small AAA after the induction of dilation of the abdominal aorta. Our data show that pharmacological inhibition of Notch signaling in small AAA attenuates its progression by not only reducing the inflammatory response but also increasing differentiation of M2-phenotype macrophages by a Tgfβ2–dependent mechanism. The abdominal aorta of *Apoe*$^{-/-}$ mice treated with DAPT also demonstrated increased contents of elastin precursors and adventitial collagen. Our findings suggest that targeting Notch signaling is a promising strategy for reducing AAA progression, particularly in those cases in which the threshold for surgical intervention for AAA has not yet been reached.

Methods

Angiotensin II Infusion and DAPT Treatment

The *Apoe*$^{-/-}$ mice (8 to 10 weeks old) were randomly divided into 4 groups: Group 1 received saline for 28 days (n=6); group 2 received AngII plus vehicle for 28 days (n=12); group 3 received AngII plus DAPT (3 days after AngII infusion, n=12); and group 4 received AngII plus DAPT (8 days after AngII infusion, n=12). Mini osmotic pumps (Model 2004; Alzet) containing AngII (1000 ng/min per kilogram) or saline were implanted subcutaneously in the neck region of anesthetized mice following standard protocol.[22] Briefly, mice were anesthetized in a closed chamber with 3% isoflurane in oxygen for 2 to 5 minutes until immobile. Each mouse was then removed and taped on a heated (35 to 37°C) procedure board with 1.0% to 1.5% isoflurane administered via nose-cone during minor surgery. Mice were injected with a Notch inhibitor, DAPT (10 mg/kg dissolved in 10% ethanol, 90% corn oil; Sigma-Aldrich), 3 times a week subcutaneously starting 3 or 8 days after the implantation of osmotic pump and continuing until completion of the study.[31] Of note, some data from group 3 (DAPT 3 days after AngII infusion) were published in our previous study.[22] All animal experiments were approved by the institutional animal care and use committee (IACUC) at the Research Institute at Nationwide Children's Hospital.

Human Infrarenal Aortic Tissue Samples

Full-thickness aortic wall tissue specimens were collected from the infrarenal abdominal aorta from patients undergoing

AAA repair operations (n=3; white men aged 67, 70, and 72 years) at the Harper University Hospital in Detroit, Michigan. Nonaneurysmal infrarenal aortic samples (n=3; white men aged 53, 53, and 78 years) were collected at autopsies. Samples were incubated in phosphate-buffered formalin and embedded in paraffin for histological analyses.[1,32,33] The human tissues were obtained after informed consent and approved by the institutional review board of Wayne State University in Detroit, Michigan.

Transabdominal Ultrasound Imaging and Quantification of Aortic Width in Mice

For in vivo imaging of the abdominal aorta in mice, 2-dimensional (B-mode) ultrasound images were obtained at weekly intervals after the implantation of osmotic pumps using a VisualSonics Vevo2100 imaging system with a mechanical transducer (MS400). After 28 days, mice were deep anesthetized with ketamine (100 mg/kg) or xylazine (20 mg/kg), and the aortas were dissected and fixed in 10% formalin. Maximum aortic diameters and total lesion area were measured using a Zeis Stemi 2000-C microscope with an Axiocam MRC camera (Carl Zeiss Microscopy), as described previously.[22] The total lesion area was defined as the visible adventitial thickening in the experimental mice at day 28 of the AngII or saline infusion and was calculated using Image-Pro Plus software.

Histology, Immunohistochemistry Quantification, and Double Immunofluorescence Staining

The abdominal aortas from the mice were embedded in paraffin, and serial sections (5 μm) were obtained. Sections were stained with hematoxylin and eosin, elastin (Sigma-Aldrich), and collagen using standard protocol.[22] Immunohistochemistry (IHC) with antibodies for tropoelastin[34] hyaluronic acid,[35] Mmp2,[36] Mmp9,[37] Cd68,[38] Mcp1,[39] Il12, Cd206,[40] Tgfβ2,[41] pSmad2,[42] NICD,[22] Hey1,[43] type 1 collagen,[44] type 3 collagen,[45] and active caspase-3[46] was performed, as described previously.[22,46,47] The details about the antibodies are provided in Table 1. Briefly, serial sections were deparaffinized, and antigen retrieval and blocking was performed. For IHC, the Vector ABC biotin kit and Vectastain DAB substrate (Vector Laboratories) were used for the development of reaction, and tissues were counterstained with hematoxylin. For double immunofluorescence, sections were incubated with

Table 1. List of Antibodies for Immunohistochemistry and Immunofluorescence

Name	Company	Cat No	Reactivity	Specificity	Dilution
Tropoelastin (p)	Abcam	ab21600	H, M	Synthetic peptide containing sequences from exons 6 to 17)	1:200
Hyaluronic acid (p)	Abcam	ab53842	H, M,	Hyaluronic acid from human umbilical cord	1:400
MMP2 (p)	Abcam	ab37150	H, M, R	Synthetic peptide corresponding to human MMP2 aa 475 to 490	1:1000
MMP9 (p)	Abcam	ab38898	H, M, R	Full length MMP9 native protein	1:1000
CD68 (m)	Abcam	ab49777	H	Carboxy terminal half of the external domain of the human CD68 molecule	1:200
Mcp1 (p)	Abcam	ab7202	M, R	Recombinant full length protein (Rat)	1:200
Il12 (m)	Gene Tex	GTX37247	M	Recombinant Murine IL12 p40	1:400
Cd206 (m)	AbD serotec	MCA2235T	M	Chimaeric CRD4-7-Fc protein	1:400
Tgfβ2 (m)	Abcam	ab36495	H, M, C	Epitope of TGFβ2 (human)	1:200
pSmad2 (p)	Cell Signaling	3108S	H, M, R	Endogenous	1:200
NICD (p)	Abcam	ab8925	H, M	Peptide: VLLSRKRRRQHGQC (aa 1755 to 1767)	1:200
Hey1 (p)	Millipore	ab5714	H, M	Recognizes Hey 1/HRT1, a Helix-loop-helix class of transcription factor	1:400
Type1 collagen (p)	Abcam	ab34710	H, R, M	Full length native protein (purified) corresponding to human collagen I aa 1 to 1464.	1:400
Type 3 collagen (p)	Abcam	ab7778	H, R, M	Full-length native protein (purified) corresponding to collagen III aa 1 to 1466	1:400
Active caspase-3 (p)	Cell Signaling	9661S	H, M, R	Endogenous levels of the large fragment (17/19 kDa) of activated caspase-3	1:200

C indicates cow; H, human; IL, interleukin; m, monoclonal; M, mouse; MMP, matrix metalloproteinase; NICD, Notch1 intracellular domain; p, polyclonal; R, rat; TGF, transforming growth factor.

antibodies for Il12, NICD, Platelet endothelial cell adhesion molecule1 (Pecam1) Pecam, smooth muscle actin, CD68, and active caspase-3 at 4°C overnight. After washing with PBS with Tween 20, the sections were immunostained with respective fluorescent secondary antibodies at room temperature for 1 hour. The slides were washed with PBS again 3 times for 45 minutes and covered by microscopic cover glass with Antifade Mounting Medium containing DAPI (Vector Laboratories) to stain nuclei. Fluorescence microscopy imaging was performed using an Olympus IX51 inverted microscope system. The total stained area in the adventitial region was quantified semiquantitatively with the Image-Pro Plus 7.0 software (Media Cybernetics), as explained previously.[48,49] Six visual fields (magnification ×400) of every lesion section were randomly included to quantify the amount of immunostaining (area of staining per total area) in the adventitial region, standardized to the average area in the control group, and to evaluate the average staining in all experimental mice. Negative control was performed by substituting primary antibody with nonspecific IgG from the same animal host as the primary antibody. Quantification of elastin fragmentation was performed using an arbitrary scale from 0 to 4, with 0 representing no visible disruption of medial elastin lamellae and 4 representing a severe transmural fragmentation of elastin structure, as described previously.[50] Calcification of aortic tissue was assessed using standard protocols for Alizarin red and von Kossa staining.[51,52] Periodic acid–Schiff (PAS) staining was performed on the intestinal tissues to assess goblet cell proliferation.

Bone Marrow–Derived Macrophage and Aorta Isolation, Polymerase Chain Reaction (PCR) Array, and Real-Time Quantitative PCR

Notch1$^{+/-}$;*Apoe*$^{-/-}$ mice were generated by crossbreeding *Apoe*$^{-/-}$ female mice in a C57BL/6J background and *Notch1*$^{+/-}$ male mice (C57BL/6J background; Jackson Laboratory, Bar Harbor, ME), as described previously.[22] Mice were kept on a 12-hour light/12-hour dark cycle with standard chow. Genotyping was performed according to the protocol from the Jackson Laboratories. The Bone marrow–derived macrophage (BMMs) were isolated from *Notch1*$^{+/-}$; *Apoe*$^{-/-}$ and *Apoe*$^{-/-}$ mice and differentiated to naïve macrophages using the standard protocol.[22] The cells were then treated with diluent, lipopolysaccharide (LPS) and interferon (IFN)-γ, or IL4, as described previously.[22] An RT^2 Profiler PCR Array (SABiosciences) was performed to determine the expression of genes involved in differentiation of naïve macrophages into either the M1 or M2 phenotype. A set of 5 housekeeping genes was included in each experiment. The relative gene expression of the genes was calculated using an online data analysis tool (http://pcrdataanalysis.sabiosciences.com/pcr/arrayanalysis.php). For activation of Tgfβ2 signaling, BMMs were treated with TGFβ2 (recombinant protein, 5 ng/mL; Sigma-Aldrich) for 48 hours prior to LPS/IFN-γ or IL4 treatment. For inactivation of Tgfβ2 signaling, BMMs were treated with TGFβ receptor kinase inhibitor (SB-431542; 10 μmol/L, Tocris Biosciences) for 48 hours prior to LPS/IFN-γ or IL4 treatment.

For mRNA expression studies of the tissue, the suprarenal aorta of ≈5 mm was cut from experimental mice at day 28 of AngII infusion and frozen in RNA*later*, and RNA was extracted using TRIzol reagent (Ambion) after homogenizing tissue with TissueLyser II (Qiagen). cDNA was synthesized using the SuperScript VILO cDNA Synthesis Kit (Invitrogen) and subjected to quantitative reverse transcriptase PCR (qRT-PCR) by SYBR Green RT-PCR kit (Applied Biosystems) using an Applied Biosystems 7500 Fast Real-Time PCR System. qRT-PCR was performed in triplicate, and fold change was determined by standardization to 18S rRNA. The expression levels were standardized against 18S rRNA using the ΔΔCt method, and mean expression of the *Apoe*$^{-/-}$ mice with saline infusion was set to 1. The primer sequences are detailed in Table 2.

Aortic Cell Isolation and Flow Cytometry

Aortic cells were isolated from the abdominal aorta of *Apoe*$^{-/-}$ mice at various intervals of time after AngII infusion. Briefly, the aortas were removed from anesthetized mice (ketamine 100 mg/kg or xylazine 20 mg/kg), minced into 3- to 4-mm pieces, and placed in 1-mL digestion solution containing 0.6 U/mL Liberase Blendzyme 3 (Roche) and 50 μg/mL porcine pancreatic elastase (Sigma-Aldrich) in DMEM media. After digestion, cells were washed in fluorescence-activated cell sorting buffer (0.5% BSA and 0.02% NaN_3 in DMEM) at 300 g for 5 minutes and subjected to fluorescence-activated cell sorting after staining with total macrophage (F4/80), M1 macrophages (Il12), and M2 macrophages (Cd206), as described previously.[22] Fluorescence-activated cell sorting studies were performed on a Becton Dickinson LSRII flow cytometer with DiVa software, and data were analyzed with Flow Jo software.

Statistical Analysis

Statistical comparisons were performed using either the Student *t* test or 1-way ANOVA followed by the Bonferroni multiple comparison test. GraphPad Prism version 5.0 was used for these comparisons, and $P<0.05$ was considered significant. Assumptions of normality and equal variance were tested and satisfied using SAS software version 9.3. The Kruskal–Wallis test was performed to determine the overall significance of the data. For multiple comparisons, a post-Bonferroni test with Holm correction (for 3 comparisons) was

Table 2. List of Primer Sequences Used in Quantitative Reverse Transcriptase Polymerase Chain Reaction Studies

Gene	Forward Primer	Reverse Primer
Mmp2	5′-GAT GTC GCC CCT AAA ACA GA-3′	5′-TGG TGT TCT GGT CAA GGT CA-3′
Mmp3	5′-TGA CGA TGA TGA ACG ATG G-3′	5′-AGA GAT GGA AAC GGG ACA AG-3′
Mmp9	5′-AGA CCT GAA AAC CTC CAA CCT CAC-3′	5′-TGT TAT GAT GGT CCC ACT TGA GGC-3′
Mmp13	5′-ATC CTG GCC ACC TTC TTC TT-3′	5′-TTT CTC GGA GCC TGT CAA CT-3′
Timp1	5′-CCA GAG CCG TCA CTT TGC TT-3′	5′-AGG AAA AGT AGA CAG TGT TCA GGC TT-3′
Timp2	5′-ACG CTT AGC ATC ACC CAG AAG-3′	5′-TGG GAC AGC GAG TGA TCT TG-3′
Timp3	5′-ATC CCC AGG ATG CCT TCT G-3′	5′-CCC TCC TTC ACC AGC TTC TTT-3′
Tgfb2	5′-GAG GCG GTG TTG TTC CAC-3′	5′-TCC TCC TTT TCT TGC TCCAG-3′
Cxcl12	5′-CTG TGC CCT TCA GAT TGT TG-3′	5′-TGG GCT GTT GTG CTT ACT TG-3′
Il5	5′-ACA TTG ACC GCC AAA AAG AG-3′	5′-ATC CAG GAA CTG CCT CGT C-3′
Il10	5′-GGT TGC CAA GCC TTA TCG GA-3′	5′-ACC TGC TCC ACT GCC TTG CT-3′
Arg1	5′-CTC CAA GCC AAA GTC CTT AGA G-3′	5′-AGG AGC TGT CAT TAG GGA CAT C-3′
iNos	5′-CTC GGA GGT TCA CCT CAC TGT-3′	5′-TCC TG TCC AAG TGC TGC AGA-3′
Notch1	5′-CCG TTA CAT GCA GCA GTT TC-3′	5′-AGC CAG GAT CAG TGG AGT TG-3′
Hey1	5′-TCT CAG CCT TCC CCT TTT C-3′	5′-CTT TCC CCT CCC TTG TTC TAC-3′
Dll4	5′-GAC CTG CGG CCA GAG ACT T-3′	5′-GAG CCT TGG ATG ATG ATT TGG-3′ -3′
Jagged1	5′-GGC TTC TCA CTC AGG CAT GAT A-3′	5′-GTG GGC AAT CCC TGT GTT TT-3′
Adam10	5′-AGC AAC ATC TGG GGA CAA AC-3′	5′-TGG CCA GAT TCA ACA AAA CA-3′
Adam17	5′-GTA CGT CGA TGC AGA GCA AA-3′	5′-GAA ATC CCA AAA TCG CTC AA-3′
Eln	5′-CTT TGG ACT TTC TCC CAT TTA TCC-3′	5′-GGT CCC CAG AAG ATC ACT TTC TC-3′
Col1a1	5′-GAG CGG AGA GTA CTG GAT CG-3′	5′-GTT CGG GCT GAT GTA CCA GT-3′
Col1a2	5′-AGG CTG ACA CGA ACT GAG GT-3′	5′-ATG CAC ATC AAT GTG GAG GA-3′
Col3a1	5′-AGG CTG AAG GAA ACA GCA AA-3′	5′-TAG TCT CAT TGC CTT GCG TG-3′

performed for the ECHO data, maximal aortic width graph, and IHC quantification. For the real-time PCR quantification, we performed the Kruskal–Wallis test using a nonparametric assay for the overall significance of the data and ordinary ANOVA followed by a Bonferroni-Holm multiple comparisons test with single-pooled variance for multiple comparisons using GraphPad Prism version 5.0. For the statistical analysis of actual incidence, Fisher's exact test was used with the SAS software. The actual incidence of the disease is defined as 50% of greater increase in the maximal aortic width compared with the control group.

Results

Pharmacological Inhibition of Notch Signaling Limits the Progression of AAA in Response to AngII

We examined the therapeutic potential of Notch inhibition on the progression of small AAA in *Apoe*$^{-/-}$ mice infused with AngII using a potent Notch inhibitor (DAPT). The *Apoe*$^{-/-}$ mice were divided into the following 4 groups: group 1 received saline for 28 days (n=6); group 2 received AngII plus vehicle for 28 days (n=12); group 3 received AngII plus DAPT (3 days after AngII infusion, n=9); and group 4 received AngII plus DAPT (8 days after AngII infusion, n=12). Mice received DAPT (10 mg/kg subcutaneously) 3 times a week for 28 days. The time points were chosen to determine the effect of Notch inhibition at the key time points of AAA progression, as suggested by previous studies by us and others.[22,53] Transabdominal ultrasound imaging (Figure 1) performed at weekly intervals starting at day 0 showed progressive increases in luminal expansion of the abdominal aorta in *Apoe*$^{-/-}$ mice in response to AngII (group 2; Figures 1B, 1F, 1J, 1N and 1R) compared with saline-treated *Apoe*$^{-/-}$ mice (group 1). Consistent with our previous studies and data from other groups, a significant increase in the luminal expansion of the abdominal aorta was observed as early as 7 days after treatment in response to AngII treatment in *Apoe*$^{-/-}$ mice (Figure 1U).[22,53,54] Significant decrease in

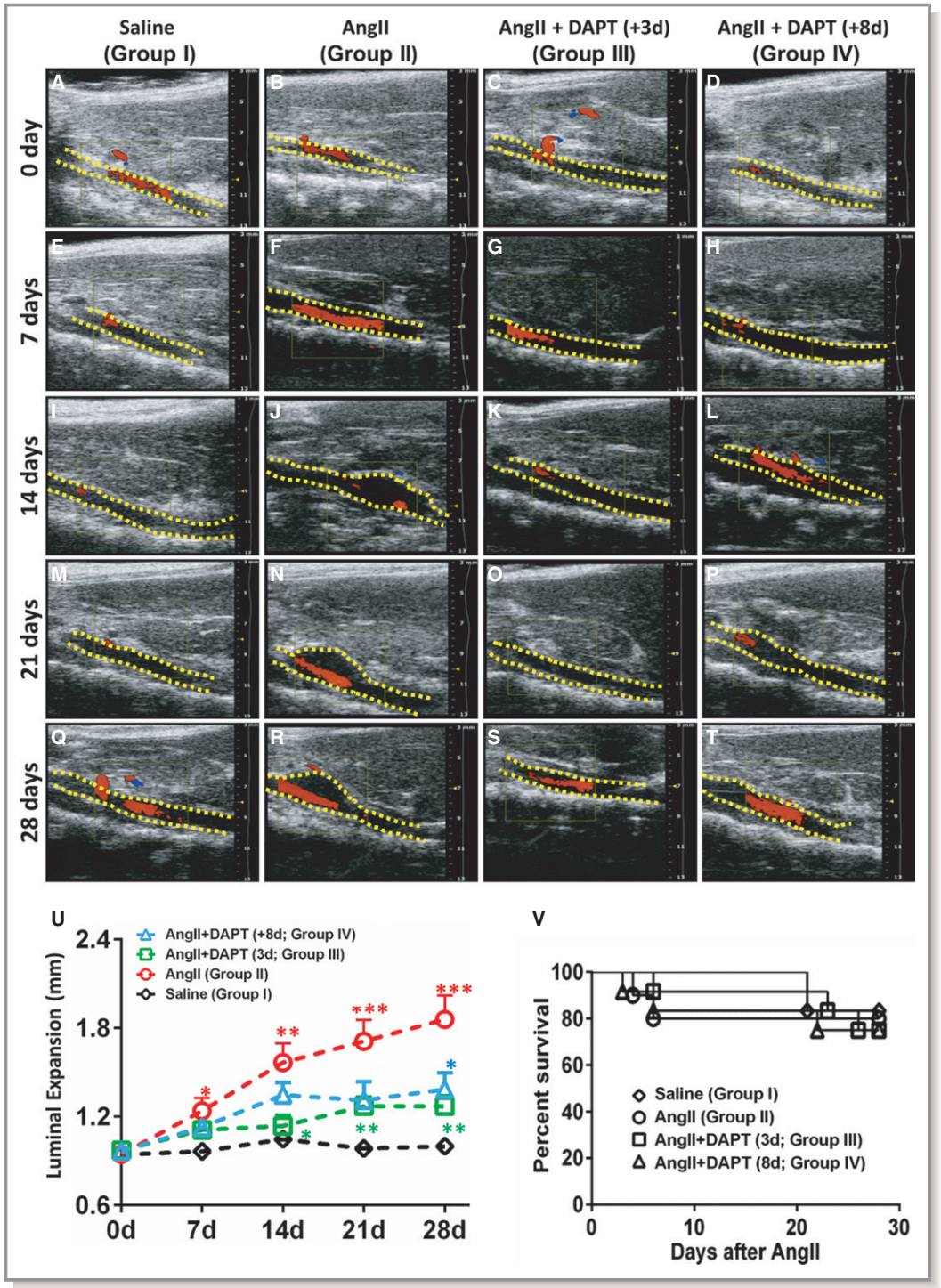

Figure 1. Pharmacological inhibition of Notch signaling limits the luminal expansion of abdominal aorta in response to AngII. A through T, Representative transabdominal ultrasound images obtained at weekly intervals using a VisualSonics Vevo2100 showing progressive increase in the luminal expansion of abdominal aorta in the *Apoe*$^{-/-}$ mice in response to saline (A, E, I, M, and Q), AngII (B, F, J, N, and R), or DAPT (10 mg/kg) started at day 3 (C, G, K, O, and S) or day 8 (D, H, L, P, and T) of AngII infusion. Dashed yellow lines outline the lumen. U, Quantification of the images demonstrating the gradual increase in luminal expansion in the abdominal aorta of each group of experimental mice (n=9). V, Survival graph showing the mortality of *Apoe*$^{-/-}$ mice in response to saline, AngII, or DAPT plus AngII during the 28-day period of the experimental protocol. $^{**}P<0.01$; $^{*}P<0.05$ (red asterisk; group 2 vs group 1, green asterisk; group 3 vs group 2, blue asterisk; group 4 vs group 2). AngII indicates angiotensin II; DAPT, N-(N-[3,5-difluorophenacetyl]-L-alanyl)-S-phenylglycine t-butyl ester.

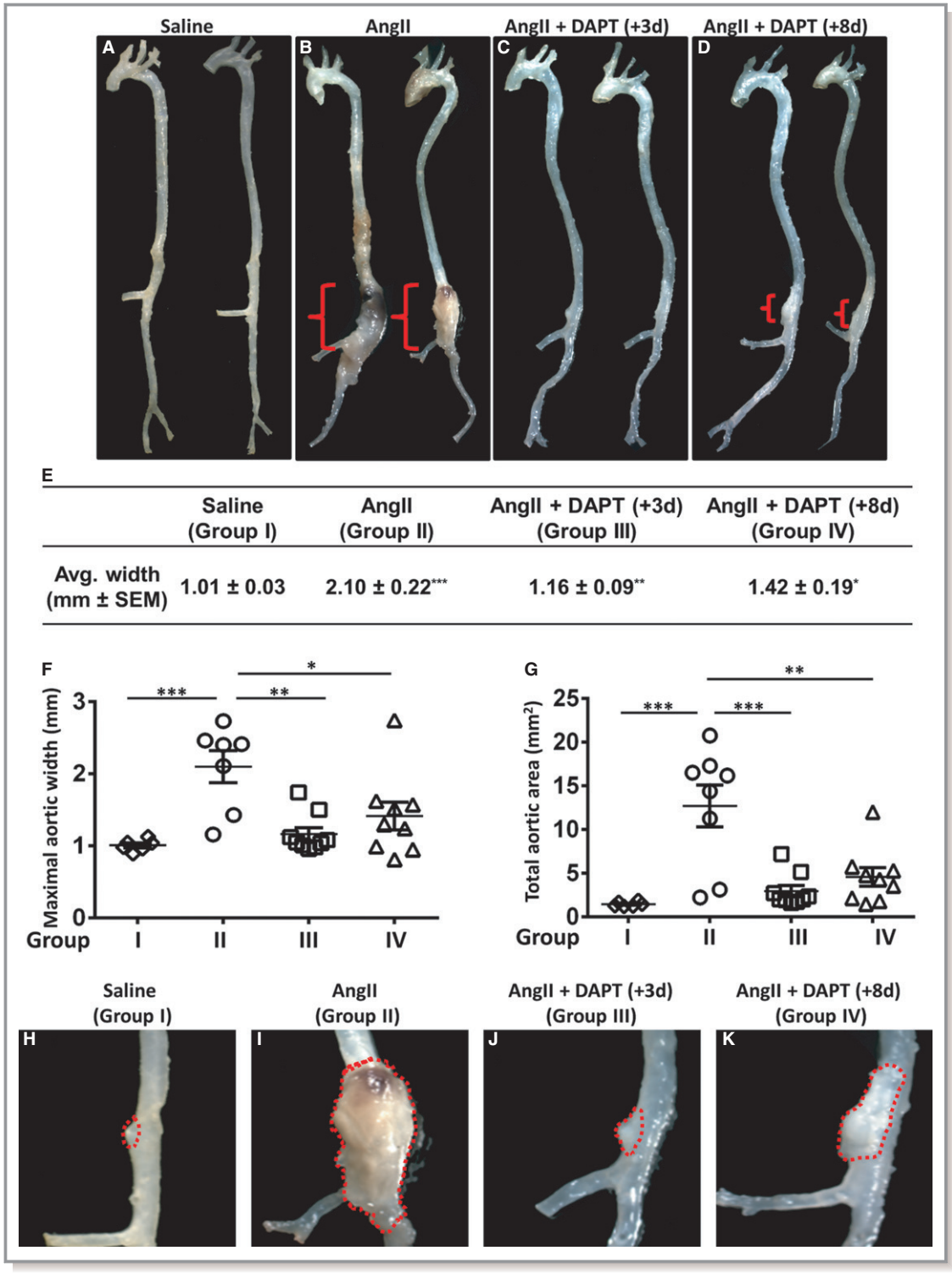

Figure 2. Pharmacological inhibition of Notch signaling reduces the maximal aortic width after 28 days of AngII infusion. A through D, Representative aortas from the experimental mice showing maximal aortic width in the suprarenal region of aorta (braces in B and D). E, Quantification of the maximal aortic width of suprarenal aorta at day 28 in *Apoe*$^{-/-}$ mice in response to saline, AngII, or DAPT treatment at day 3 or day 8 of AngII infusion, using a Zeis Stemi 2000-C microscope. F and G, Quantification of the maximal aortic width and total aneurysmal area of abdominal aorta from experimental mice at day 28 (details described under Methods). H through K, Representative images showing the aneurysmal area in experimental mice. Results are represented as mean±SEM; each symbol represents an individual mouse at day 28. ***P<0.001; **P<0.01; *P<0.05. AngII indicates angiotensin II; DAPT, N-(N-[3,5-difluorophenacetyl]-L-alanyl)-S-phenylglycine t-butyl ester.

the luminal expansion of the abdominal aorta was observed in *Apoe*$^{-/-}$ mice with DAPT treatment started at day 3 (group 3) at days 14, 21, and 28 compared with group 2 (Figure 1C, 1G, 1K, 1O, and 1S).[22] Although a marginal but insignificant increase in the luminal expansion was observed until day 14 in *Apoe*$^{-/-}$ mice treated with DAPT started 8 days after the AngII infusion (group 4), no further progression of luminal expansion was observed in this group (Figure 1D, 1H, 1L, 1P, and 1T). The luminal expansion at day 28 was significantly less in group 4 compared with group 2 (Figure 1U). No significant difference in luminal expansion was observed in groups 3 and 4 compared with group 1 at any time interval (Figure 1U). Treatment by the Notch inhibitor did not affect survival of these mice over the 28-day course of the studies (Figure 1V). These findings suggest that Notch inhibition at an early stage of the disease reduced the progressive increase in luminal expansion that occurs with AngII infusion.

The macroscopic examination of aortas at day 28 demonstrated a significantly increased maximal aortic width in response to AngII in group 2 (2.10±0.22 mm; Figure 2A, 2B, 2E, and 2F) compared with saline-treated group 1 (P<0.001; 1.0±0.03 mm). No increase in the maximal aortic width was observed in group 3 treated with DAPT started at day 3 of AngII infusion (1.16±0.09 mm; Figure 2C, 2E, and 2F) such that aortic width was significantly less compared with group 2 (P<0.01). Marginal increase in the aortic width was observed in group 4 treated with DAPT started at day 8 of AngII infusion (1.42±0.19 mm; Figure 2D through 2F) but was significantly less than group 2 treated with AngII alone (P<0.05). Consistent with maximal aortic width data, the total lesion area covered by the aneurysmal growth was also significantly decreased by Notch inhibitor in both these treatment groups compared with AngII alone (P<0.01; Figure 2G through 2K). Consistent with transabdominal ultrasound imaging data (Figure 1), these results confirm the preventive effects of Notch inhibition on the increase of maximal aortic diameter that occurs with AngII infusion.

Histological examination of hematoxylin and eosin–stained paraffin sections of aorta demonstrated clear differences in the medial and adventitial layers between the DAPT-treated mice and non–DAPT-treated mice (Figure 3A through 3L). *Apoe*$^{-/-}$ mice treated with AngII alone demonstrated cellular

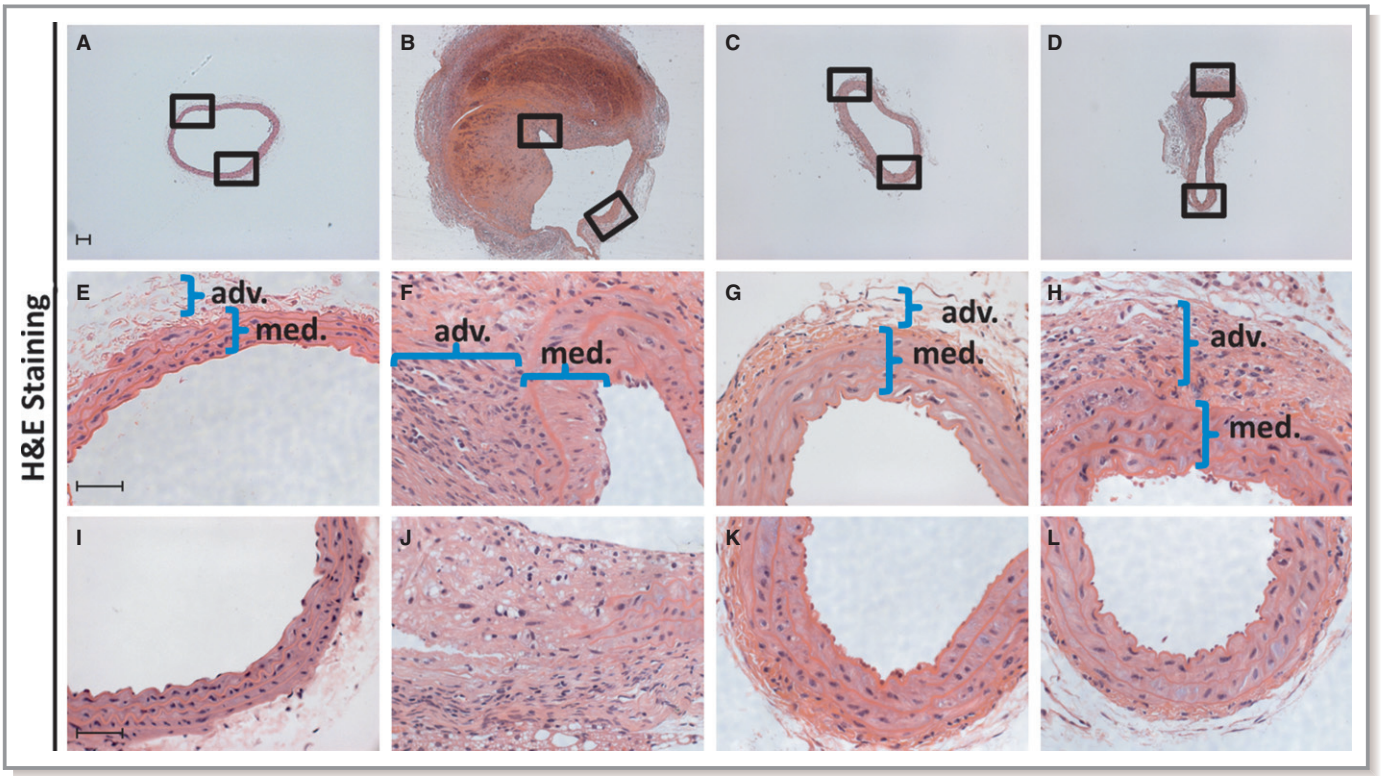

Figure 3. Pharmacological inhibition of Notch signaling attenuates extent of AAA progression in an AngII-induced mouse model of AAA. A through L, Transverse sections of abdominal aorta stained with H&E (n=6 for each group) illustrating the extent of AAA progression at day 28 in response to saline (A, E, and I), AngII (B, F, and J), or DAPT treatment at day 3 (C, G, and K) or day 8 (D, H, and L) of AngII. Scale=1 mm (A through D) and 50 μm (E through L). Images E through L are the magnified views of the 2 different regions highlighted in the boxes in A through D. Braces in E through H indicate the thickness of medial and adventitial layers. ***P<0.001; **P<0.01; *P<0.05. AAA indicates abdominal aortic aneurysm; adv, adventitia; AngII, angiotensin II; DAPT, N-(N-[3,5-difluorophenacetyl]-L-alanyl)-S-phenylglycine t-butyl ester; H&E, hematoxylin and eosin; med, media.

and architectural changes of typical AAA including thrombus formation, adventitial remodeling, inflammatory cell infiltration, and elastin fragmentation (Figure 3B, 3F, and 3J). The aortas from group 3 treated with DAPT started at day 3 of AngII infusion displayed a well-defined lumen with no elastin fragmentation and minimal infiltration of inflammatory cells (Figure 3C, 3G, and 3K). Despite marginal thickening in group 4, DAPT treatment started at day 8 of AngII infusion prevented disruption of the elastic lamellae, and no other characteristic features of AAA were observed in this group (Figure 3D, 3H, and 3L). These findings suggested that Notch inhibition not only prevented the progressive growth of small AAA but also suppressed the characteristic traits of AAA.

DAPT Decreases the Expression of Notch Signaling in the Abdominal Aorta of *Apoe*$^{-/-}$ Mice

Consistent with our previous studies, a robust increase in the nuclear staining of NICD and its downstream target Hey1 was observed in the adventitial layer of group 2 in response to AngII compared with saline-treated group 1 (Figure 4A through 4H). As expected, DAPT prevented activation of Notch signaling, as demonstrated by a near absence of nuclear NICD in groups 3 and 4 (Figure 4A through 4H). Significant increase in the mRNA expression of *Notch1*; its upstream ligands, *Jagged1* and *Dll4*; and its downstream target *Hey1* was observed in the aortas of group 2 mice versus group 1 (Figure 4I through 4L). The mRNA expression of *Jagged1*, *Dll4*, and *Hey1* in groups 3 and 4 decreased with DAPT treatment compared with group 2 and were comparable to group 1 (Figure 4I through 4L). The mRNA expression of a disintegrin and metalloproteases (ADAMs) 10 and 17, which cause a proteolytic cleavage leading to the release of the intracellular domain of Notch1 (NICD), were also markedly increased in group 2 compared with group 1 and were significantly downregulated by Notch inhibition in groups 3 and 4 ($P<0.01$; Figure 4M and 4N). Dose-dependent decrease in *Hey1* expression was also observed in the ex vivo BMM cell culture isolated from *Apoe*$^{-/-}$ mice (Figure 4O). The data demonstrated inhibition of several members of the Notch signaling pathway by DAPT and also suggested an active role for the Notch signaling pathway in the progression of aortic aneurysms.

DAPT-Induced Stabilization of AAA is Associated With Increased Synthesis of Elastin Precursors

Activation of MMPs and fragmentation of elastin have been suggested as biomarkers for AAA progression.[55,56] Consequently, we evaluated whether Notch inhibition provides stability to the aneurysmal tissue by altering these characteristic features of the aneurysmal tissue. We particularly focused on the areas of marginal thickening in the abdominal aorta from DAPT-treated *Apoe*$^{-/-}$ mice for better understanding of the alterations caused by Notch inhibition with regard to AAA stability (brackets in Figure 3E through 3H). Marked fragmentation of elastic fibers was observed in AngII-treated group 2 compared with saline-treated group 1 ($P<0.001$; Figure 5A, 5B, and 5Y). Occasional elastin fragmentation was also observed in group 4 treated with DAPT started 8 days after the AngII infusion but was significantly less compared with group 2 (Figure 5D and 5Y). No detectable elastin degradation was observed in group 3 treated with DAPT started 8 days after the AngII infusion (Figure 5C and 5Y). Quantification of the elastin fragments revealed a 3.5-fold increase in the elastin fragmentation in group 2 compared with only 1.5-fold in group 4 ($P<0.05$; Figure 5Y). Elastin fibers are formed by crosslinking of the soluble protein tropoelastin, which provides architectural stability to the aorta. Negligible immunostaining of tropoelastin was observed in the saline-treated *Apoe*$^{-/-}$ mice (Figure 5E). A marginal but insignificant increase in tropoelastin immunostaining was observed in group 2 treated with AngII alone and group 3 treated with DAPT started 3 days after the AngII infusion (Figure 5F and 5G). Robust increases in tropoelastin immunostaining were observed in the abdominal aorta from group 4 treated with DAPT started 8 days after the AngII infusion compared with group 2 (Figure 5H). The mRNA expression of tropoelastin in response to AngII increased by 6-fold in group 2 compared with group 1 ($P<0.01$; Figure 5Z). A similar increase in the mRNA expression of tropoelastin was also observed in group 4 and was comparable to group 2 (Figure 5Z). Tropoelastin expression was also increased by ≈3.5-fold in group 3 compared with group 1 but was significantly less than group 2 or group 4 ($P<0.05$; Figure 5Z). Hyaluronic acid is an important elastogenic factor secreted by smooth muscle cells and plays a key role in the elastic fiber assembly through binding with elastin-associated proteins including tropoelastin. Increased immunostaining of hyaluronic acid was observed in the medial aortic layer of groups 3 and 4 compared with group 2 (Figure 5I through 5L). Increased collagen content was observed in the aortas of groups 3 and 4 compared with group 2 and was predominant in the adventitial region (Figure 5M through 5P). The IHC also showed increased immunostaining of type III collagen in group 4 compared with group 2 (Figure 5U through 5X), whereas the expression of type I collagen was similar in group 4 compared with group 2 (Figure 5Q through 5T). The mRNA expression of collagen I-α1 (*Col1a1*), collagen-α2 (*Col1a2*), and collagen III (*Col3a1*) was increased by almost 20-fold in response to AngII in group 2 compared with group 1 (Figure 5AA through 5AC). The *Col1a1*, *Col1a2*, and *Col3a1* mRNA levels were also increased

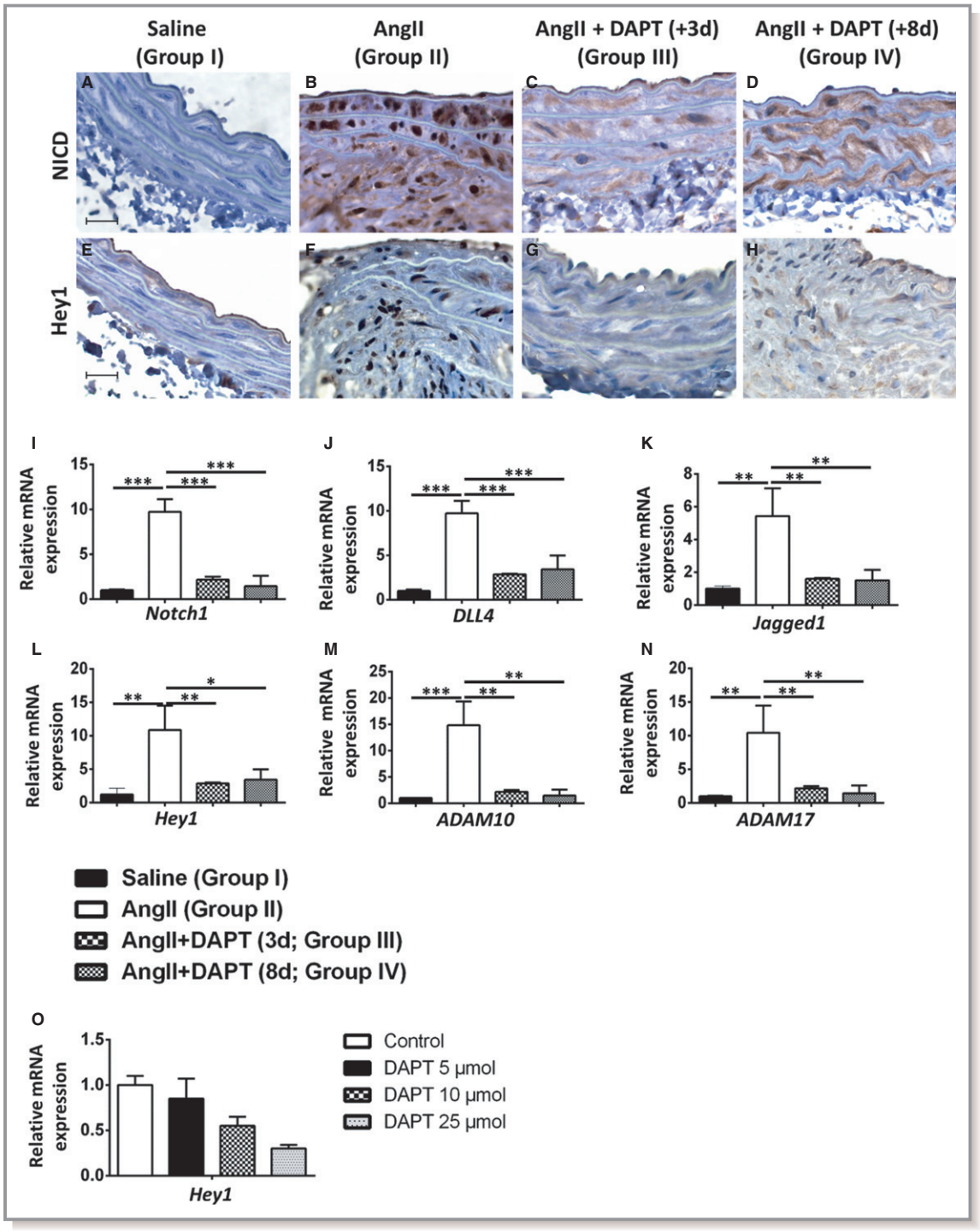

Figure 4. AngII infusion increases Notch1 signaling in the abdominal aorta of *Apoe*$^{-/-}$ mice were prevented by DAPT treatment. A through H, Representative images of IHC using antibodies against NICD (A through D) or Hey1 (E through H) in the abdominal aorta of *Apoe*$^{-/-}$ mice treated with saline, AngII, or DAPT at day 3 or day 8 of AngII. I through N, Quantification of RT-PCR demonstrating mRNA expression of *Notch1* (I), its upstream ligands *Jagged1* (J) and *Dll4* (K) and its downstream target *Hey1* (L), and its activators *Adam10* (M) and *Adam17* (N) in the abdominal aorta of experimental mice. The results were standardized to 18S rRNA and reported as ratio (mean±SEM, n=3 for each group) to saline-treated mice. O, Quantification of RT-PCR demonstrating mRNA expression of *Hey1* in the BMDM of *Apoe*$^{-/-}$ mice in response to various concentrations of DAPT. Scale bars=50 μm (A through H). ***P<0.001; **P<0.01; *P<0.05. AngII indicates angiotensin II; BMDM, bone marrow–derived macrophages; DAPT, N-(N-[3,5-difluorophenacetyl]-L-alanyl)-S-phenylglycine t-butyl ester; IHC, immunohistochemistry; NICD, Notch1 intracellular domain; RT-PCR, reverse transcriptase polymerase chain reaction.

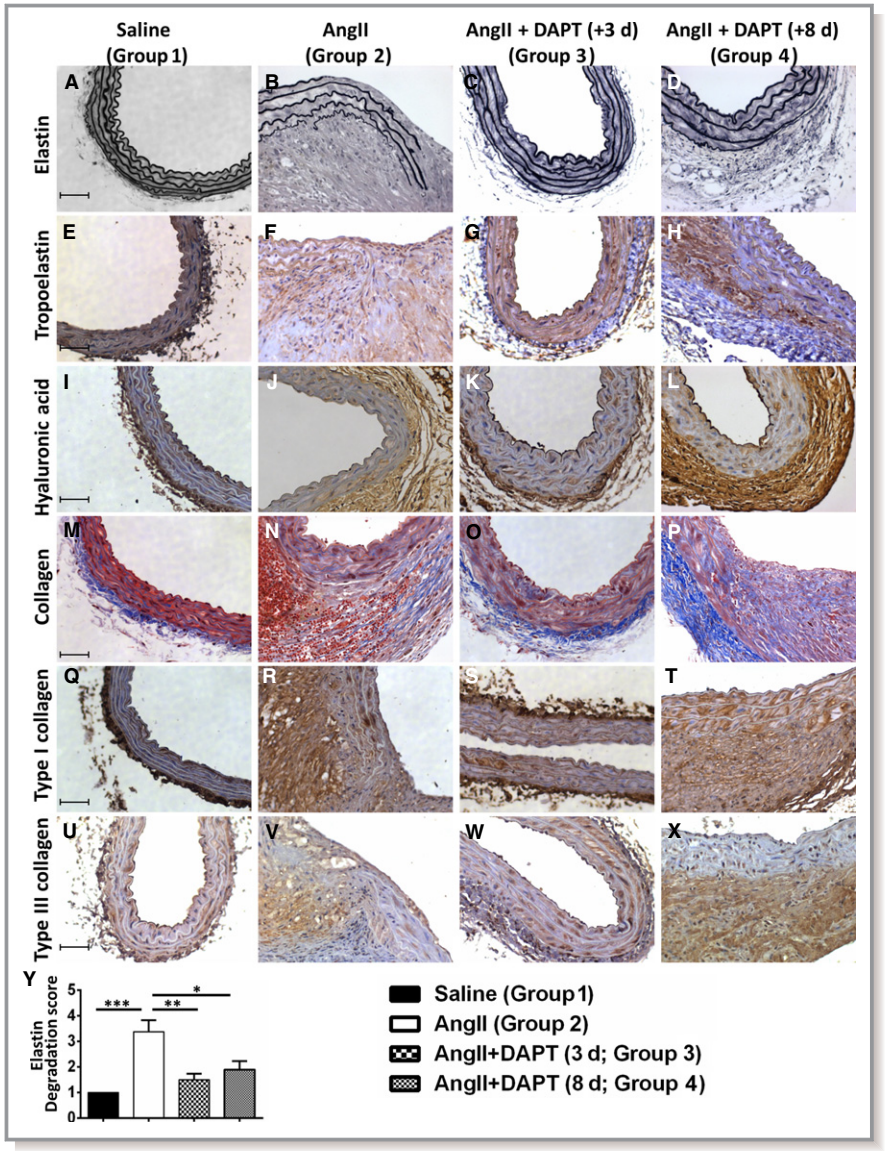

Figure 5. Notch inhibition–induced stabilization of AAA is associated with increased synthesis of elastin precursors. A through D, Representative images of elastin staining demonstrating the extent of elastin fragmentation in *Apoe*$^{-/-}$ mice infused with saline, with AngII alone, or with DAPT at day 3 or day 8 of AngII. Representative images of IHC staining of abdominal aorta from respective experimental groups with antibodies against tropoelastin (E through H) and hyaluronic acid (I through L) as markers of elastin precursors. M through P, Collagen contents in the abdominal aorta of experimental groups visualized in blue using trichrome staining. Q through X, Increased expression of type III collagen in the aneurysmal aorta of AAA in response to AngII. A through H, Representative images of IHC using antibodies against type I collagen (Q through T) or type III collagen (U through X) in the adventitial region of abdominal aorta of *Apoe*$^{-/-}$ mice treated with saline, AngII, or DAPT treatment at day 3 or day 8 of AngII. Y, Semiquantitative analysis of elastin fragmentation score using an arbitrary scale from 0 to 4, with 0 representing no visible disruption of medial elastin lamellae and 4 representing a severe transmural elastin fragmentation (details described under Methods). Total RNA were isolated from equal-length abdominal aorta and subjected to qRT-PCR. Shown in the figure (Z through AC) are qRT-PCR results using primers for tropoelastin (*Eln*), *Col1a1*, *Col1a2*, and *Col3a1* standardized to 18S rRNA and reported as ratio (mean±SEM, n=3 for each group) to saline treated mice. Scale bar=50 μm in A through P. ***P<0.001; **P<0.01; *P<0.05. AAA indicates abdominal aortic aneurysm; AngII, angiotensin II; DAPT, N-(N-[3,5-difluorophenacetyl]-L-alanyl)-S-phenylglycine t-butyl ester; IHC, immunohistochemistry; qRT-PCR, quantitative reverse transcriptase polymerase chain reaction.

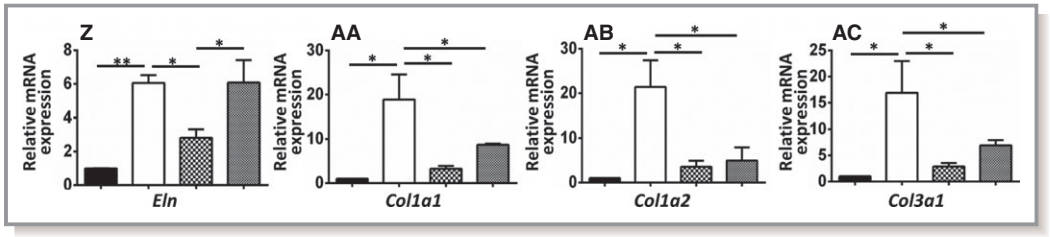

Figure 5. Continued

marginally in the aortas of DAPT-treated groups 3 and 4 (≈4-fold) but were significantly less than in group 2 ($P<0.05$; Figure 5AA through 5AC). The integrity of the endothelial layer was examined in the experimental aortas by double immunostaining with PECAM and anti-α-smooth muscle actin (Figure 6A through 6P). A clear loss of endothelial cell layer was observed in the areas of elastin fragmentation in group 2 (Figure 6B). No such breaks in the endothelial cell layers were observed in group 3 or group 4, suggesting preventive effects of Notch inhibition on the loss of endothelial cell layer (Figure 6C, 6D, 6K, and 6L). The data suggested that Notch inhibition may lead to the stabilization of the aneurysmal aorta associated with regeneration of elastin precursors and reduction in collagen degradation.

DAPT-Induced Stabilization of AAA is Associated With Decreased Proteolytic MMPs and Reduced Ratio of MMPs to Tissue Inhibitors of Metalloproteinases

Excessive MMP activation causes degradation of the elastin and interstitial collagenous matrix of the medial layer of aorta. We next examined whether the preventive effects of Notch inhibitor on AAA progression are associated with decreased MMP expression. Our data demonstrated a marked increase in the mRNA expression of *Mmp2*, *Mmp3*, *Mmp9*, and *Mmp13* in the aorta of *Apoe*$^{-/-}$ mice in response to AngII in group 2 (Figure 7A through 7D). The expression of these MMPs was significantly decreased by the Notch inhibitor in groups 3 and 4 ($P<0.01$; Figure 7A through 7D). The balance between MMPs and their physiological inhibitors tissue inhibitors of metalloproteinases (TIMPs) determines the activity and potential of the MMPs to degrade extracellular matrix components. The *Timp1* and *Timp2* mRNA levels were increased by 20- and 4-fold, respectively, in group 2 compared with group 1 (Figure 7E and 7F), whereas expression of *Timp1* and *Timp2* in groups 3 and 4 increased only ≈2-fold compared with group 1 and were significantly lower than group 2 ($P<0.05$). The expression of *Timp3* was moderately increased by AngII infusion and was comparable among groups 2, 3, and 4 (Figure 7G), such that the relative ratios of *Mmp2* to *Timp3* and *Mmp9* to *Timp3* were significantly lower in DAPT-treated groups 3 and 4 compared with group 2 ($P<0.05$; Figure 7H and 7I). Protein expression of Mmp2 and Mmp9 was also decreased significantly by Notch inhibitor in these experimental animals, as determined by IHC followed by semiquantitative analysis of the adventitial layer of aorta (Figure 7J through 7S). The data demonstrated a robust increase in the proteolytic MMPs and imbalance in the MMP-to-TIMP ratio in the macrophage-rich adventitial layer of the abdominal aorta in a mouse model of AngII and its subsequent reduction by Notch inhibition. Studies have shown that disruption of the Notch signaling pathway by gene deletion or γ-secretase inhibitor induces mucosecreting goblet cell conversion of crypt proliferative cells in the intestine.[57] Indeed, we detected increases in the size and number of goblet cells in the crypts of intestinal tissue in DAPT-treated *Apoe*$^{-/-}$ mice (Figure 8A through 8H). Previously, we also demonstrated that deficiency of Notch1 promotes calcification in an in vitro primary aortic valve cell culture system.[51,52] No changes in the calcium contents of aortic tissue were observed in these experimental groups in response to DAPT, suggesting that these effects of Notch1 signaling on calcification may be cell dependent (Figure 8I through 8P).

Notch Inhibition Decreases M1-Differentiated Macrophages and Increases M2-Differentiated Macrophages in the Abdominal Aorta of *Apoe*$^{-/-}$ Mice in Response to AngII

Macrophage infiltration in response to AngII is an important step in AAA formation and progression in the AngII mouse model of AAA. First, we examined whether progression of AAA in *Apoe*$^{-/-}$ mice in response to AngII is accompanied by alterations in the M1 or M2 differentiation of naïve macrophages and their preferential influx. Flow cytometry (fluorescence-activated cell sorting) was performed on aortic cell suspensions in the abdominal aorta of *Apoe*$^{-/-}$ mice infused with AngII at various time intervals (days 0, 3, 7, 14, 21, and 28) using F4/80, Il12, and Cd206 surface markers to highlight total and M1- and M2-differentiated macrophages, respectively. In untreated *Apoe*$^{-/-}$ mice, total macrophages (stained with F4/80) contributed to less than 10% of the total aortic cell population and were primarily negative

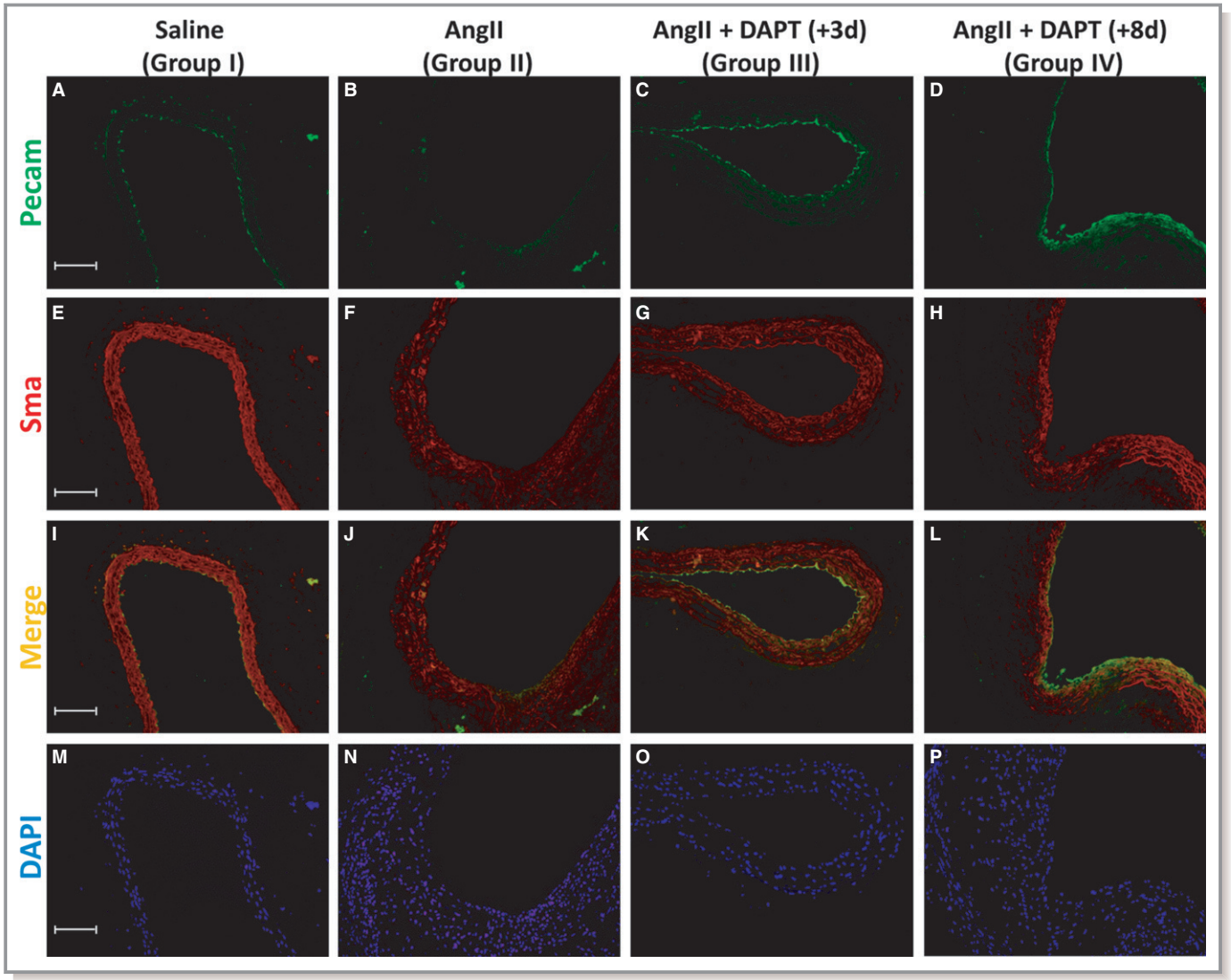

Figure 6. Notch inhibition maintains the integrity of the endothelial layer in *Apoe*$^{-/-}$ mice treated with AngII. A through H, Double immunofluorescence staining demonstrating coexpression of Pecam (A–D; green) and Sma (E–H; red) in the abdominal aorta of *Apoe*$^{-/-}$ mice treated with saline, AngII, or DAPT at day 3 or day 8 of AngII. Merged images of the immunofluorescence staining are shown (I through L). Aortas from 3 mice were examined, and representative sections are shown. Scale bar=50 μm. All nuclei were stained by DAPI (blue; M through P). AngII indicates angiotensin II; DAPI, 4′,6-diamidino-2-phenylindole; DAPT, N-[N-(3,5-Difluorophenacetyl)-L-alanyl]-S-phenylglycine t-butyl ester; Sma, smooth muscle actin.

for Il12 staining (Figure 9A and 9B). In response to AngII, the total population of macrophages increased to 27% of all aortic cells within 3 days, peaked at ≈40% at day 7, and remained constant thereafter until completion of the study (Figure 9A). The majority of infiltrated macrophages in response to AngII were positive for Il12 staining (≈30%), suggesting their M1 differentiation (P<0.001; Figure 9B). In contrast, the Cd206-positive M2 macrophages decreased from 10% in the abdominal aortas of untreated *Apoe*$^{-/-}$ mice to ≈2% within 3 days of AngII treatment (Figure 9B). This resulted in an increased ratio of M1 to M2 macrophages in response to AngII in these mice (P<0.01). Thus, the data suggested that the infiltration of M1-differentiated macrophages likely occurs at early stages of AAA development at the expense of M2 macrophages.

Previously, we documented the *in vitro* roles for *Notch1* haploinsufficiency in promoting the M2 phenotype of macrophages.[22] In this study, we determined whether pharmacological inhibition of Notch can alter the differentiation of macrophages in a mouse model of AAA after the disease is established. The sections from abdominal aorta were stained with CD68 and Mcp1 to examine the total macrophage content and their inflammatory component in response to AngII. IHC demonstrated a robust increase in *CD68* staining in the aortas of AngII-treated group 2, compared with saline-treated group 1, that was primarily localized in the adventitial layer and was

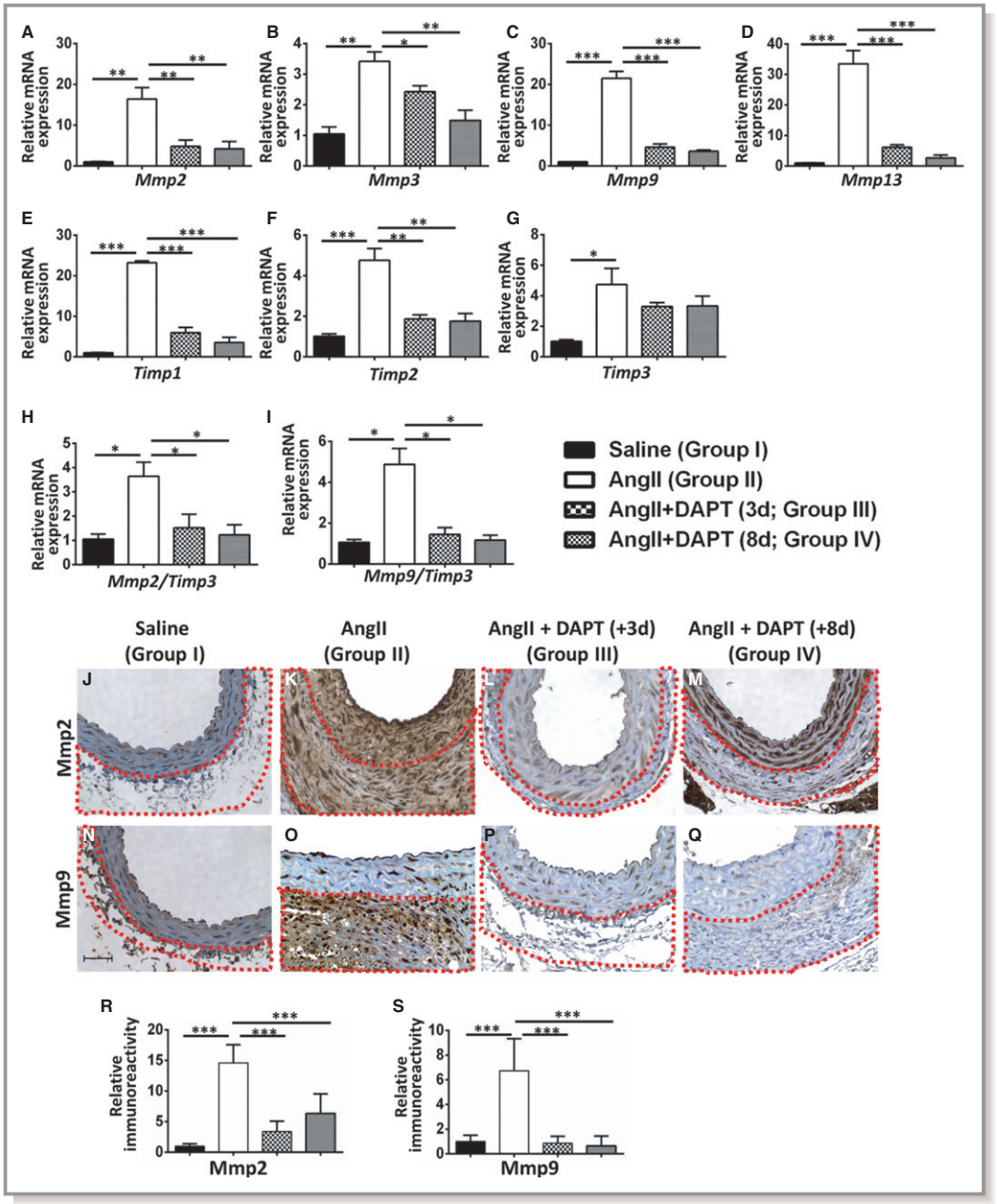

Figure 7. Notch inhibition–induced stabilization of AAA is associated decreased proteolytic MMPs and reduced *MMP*-to-*TIMP* ratio. A through D, qRT-PCR data showing the mRNA expression of *Mmp2*, *Mmp3*, *Mmp9*, and *Mmp13* at day 28 in the abdominal aorta of *Apoe*$^{-/-}$ mice infused with saline, AngII, or DAPT treatment at day 3 or day 8 of AngII. E through G, qRT-PCR data showing the mRNA expression of *Timp1*, *Timp2*, and *Timp3* in the experimental mice at day 28. The results were normalized to 18S rRNA and reported as the ratio (mean±SEM, n=3 for each group) to saline-treated mice. H and I, Ratio of *Mmp2* to *Timp3* and *Mmp9* to *Timp3* expression in the experimental mice at day 28 as a measure of net increase in the activation of Mmp2 and Mmp9 in the experimental groups. J through Q, Representative images of IHC using antibodies against Mmp2 (J through M) or Mmp9 (N through Q) in the adventitial region of abdominal aorta of *Apoe*$^{-/-}$ mice treated with saline, AngII, or DAPT treatment at day 3 or day 8 of AngII. Dashed red lines outline the adventitial layer. R and S, Semiquantitative analysis of Mmp2 and Mmp9 IHC using Image-Pro Plus software. Six visual fields (magnification ×400) of every lesion section were randomly included to quantify the amount of immunostaining (area of staining per total area) standardized to the average area in the control group. Scale bar=50 μm (J and Q). ***P<0.001; **P<0.01; *P<0.05. AAA indicates abdominal aortic aneurysm; AngII, angiotensin II; DAPT, N-(N-[3,5-difluorophenacetyl]-L-alanyl)-S-phenylglycine t-butyl ester; IHC, immunohistochemistry; MMPs, matrix metalloproteinases; qRT-PCR, quantitative reverse transcriptase polymerase chain reaction; TIMP, tissue inhibitor of metalloproteinases.

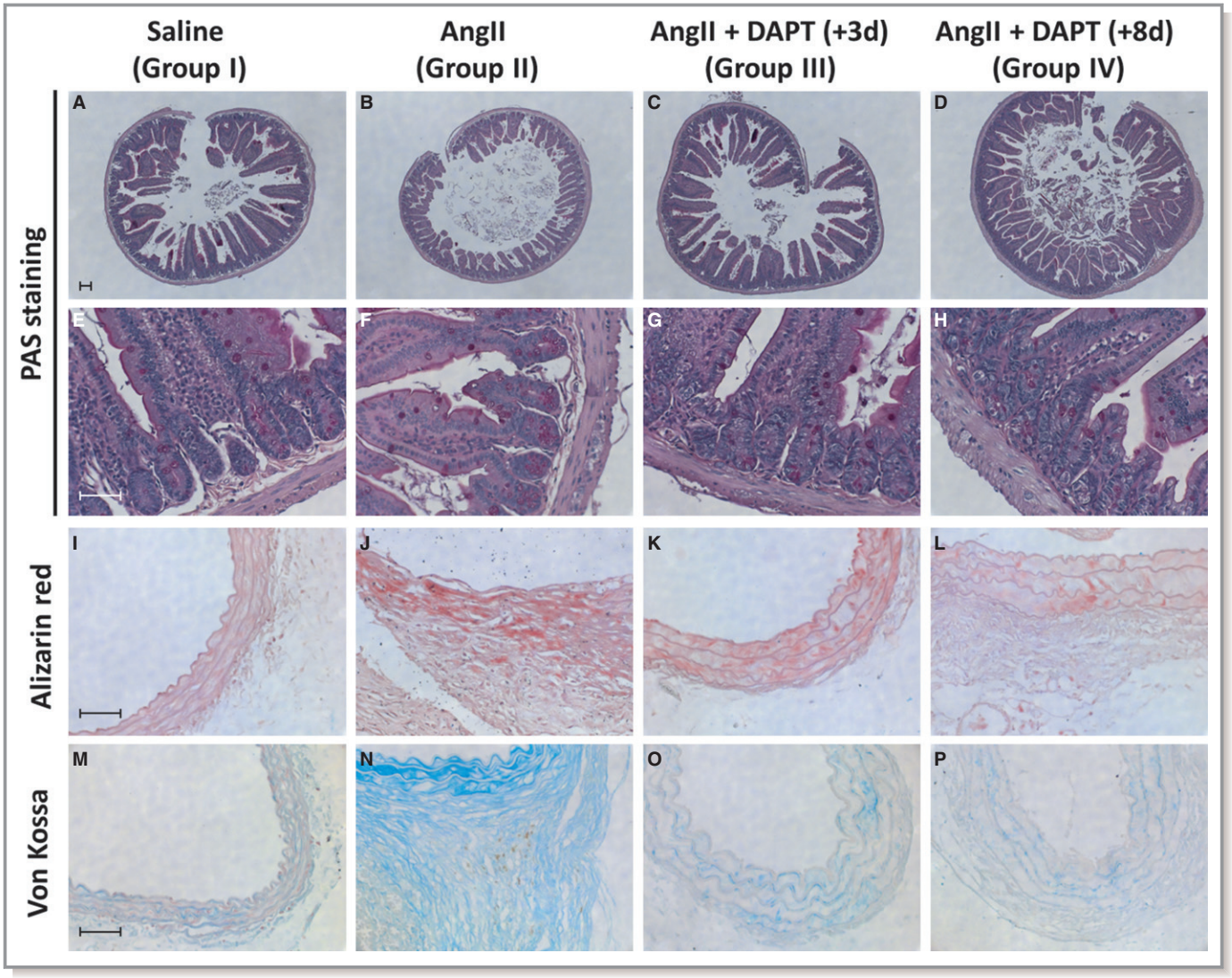

Figure 8. DAPT increases goblet cells in the crypts of intestinal tissue in DAPT-treated *Apoe*$^{-/-}$ mice but does not induce calcification of aortic tissue. A through H, Representative images with PAS staining showing the goblet cells (dark pink) and thickening of intestinal crypts. I through L, Representative images with Alizarin red staining and (M through P) von Kossa staining for calcium contents of aortic tissue in the experimental groups. Scale=1 mm (A through D) and 50 μm (E through P). AngII indicates angiotensin II; DAPT, N-(N-[3,5-difluorophenacetyl]-L-alanyl)-S-phenylglycine t-butyl ester; PAS, Periodic acid–Schiff.

highly associated with Mcp1 immunostaining (Figure 10A, 10B, 10E, and 10F). Marginal Cd68 staining was also observed in group 4 treated with DAPT started day 8 of AngII infusion but was considerably less than group 2 (Figure 10D and 10Q). Interestingly, the marginal increase in CD68 content in the DAPT-treated *Apoe*$^{-/-}$ mice in the adventitial region was not associated with Mcp1 expression (Figure 10H and 10R). No increase in CD68 or Mcp1 content was observed in group 3 treated with DAPT started day 3 of AngII infusion (Figure 10C, 10G, 10Q, and 10R). To examine whether the preventive effects of Notch inhibitor on AAA progression are associated with changes in M1 or M2 macrophages, we subjected abdominal aortic tissue from our experimental mice for immunostaining using Il12 to stain M1 macrophages and Cd206 to identify M2 macrophages. As shown in Figure 10I through 10L, significantly increased Il12 staining was observed in the adventitial region of the abdominal aorta in response to AngII in group 2 and was markedly reduced by Notch inhibitor in groups 3 and 4 (Figure 10S). In contrast, significantly increased Cd206 staining was observed in the adventitial region of the abdominal aorta in group 4 treated with DAPT started day 8 of AngII infusion compared with group 2 treated with AngII alone (Figure 10M through 10P, and 10T). No differences in Il12 or Cd206 staining were observed in groups 1 and 3, likely due to a lack of macrophages (Figure 10I, 10K, 10M, 10O, 10S, and 10T). Furthermore, staining with active caspase-3 revealed increased apoptosis in the medial and adventitial layer of group 2 (Figure 11A through 11D). Marginal active caspase-3

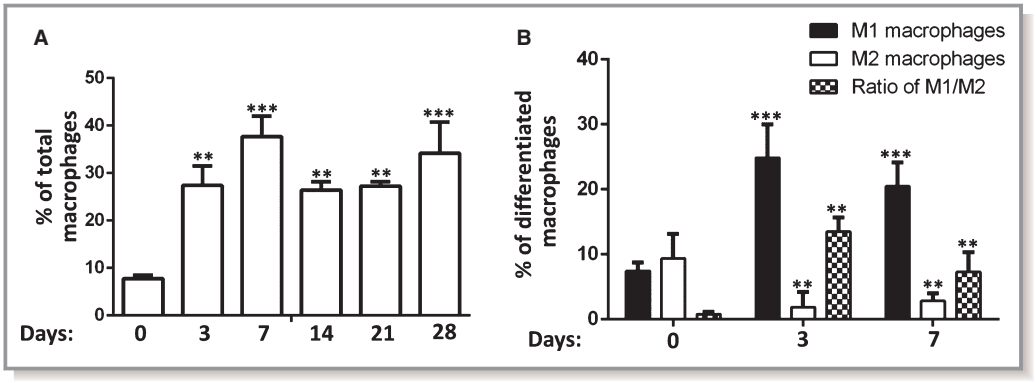

Figure 9. The progression of AAA in AngII-induced *Apoe*$^{-/-}$ *mice* model is associated with derangements in the M1 and M2 macrophages at the site of vascular injury. Aortic cells extracted from abdominal aortas were analyzed by flow cytometry at 0, 3, 7, 14, 21, and 28 days of AngII treatment. A, Quantification of the influx of total macrophages in the abdominal aorta of *Apoe*$^{-/-}$ mice at various time intervals from day 0 to day 28 of AngII infusion, as determined by flow cytometry. B, Differential staining of the aortic cell suspension using F4/80 for total macrophages, Il12 for M1 macrophages, and Cd206 for M2 macrophages. All values are expressed as mean±SEM (n=4). ***P<0.001; **P<0.01. AAA indicates abdominal aortic aneurysm; AngII, angiotensin II.

staining was observed in the medial layer of aortas with DAPT treatment in groups 3 and 4. Marginal active caspase-3 staining was observed in the macrophage-containing adventitial layer in group 4, as validated by double immunostaining showing the coexpression of active caspase-3 staining in the CD68-positive macrophages in group 4 (arrow heads in Figure 11P). Interestingly, active caspase-3 staining in the adventitial layer of group 2 was not highly coexpressed with CD68-positive macrophages (arrow heads in Figure 11N) and was primarily concentrated in the smooth muscle cell–rich medial layer.

The data suggested that Notch inhibition is associated with decreased M1 macrophages and increased M2 macrophages at the site of vascular injury and indicated that M2 differentiation of macrophages may render them incompetent to infiltrate and participate in the propagation of inflammation. The data also demonstrated an overall imbalance of the M1-to-M2 ratio in the mouse model of AAA.

Notch Activation in Human AAA Correlates Strongly With M1-Differentiated Macrophages

Next, we examined whether human AAA is also associated with a similar predominance of M1 macrophages in the abdominal aorta (Figure 12A through 12L). Double immunofluorescence staining with a standard marker for M1 macrophages (IL12) and active Notch1 signaling (NICD) demonstrated negligible staining for IL12-positive macrophages or NICD in the abdominal aortas obtained from control subjects (Figure 12A, 12D, and 12G). The immunostaining of IL12-positive macrophages was substantially stronger in the infrarenal aortas from AAA patients (Figure 12B and 12C) and was found to be coexpressed with active Notch1 signaling (Figure 12E, 12F, 12H, and 12I). Consequently, the data demonstrated increased content of M1 macrophages in the human AAA, suggesting a close association between active Notch1 signaling and M1 polarization of macrophages.

Notch1 Deficiency Promotes M2 Differentiation by Upregulating Tgfβ2 Signaling in the Macrophages and Aortas of *Apoe*$^{-/-}$ Mice in Response to AngII

To identify the potential pathways by which Notch signaling regulates macrophage differentiation in AAA, we performed an unbiased screen of cytokines and chemokines using the RT^2 Profiler PCR Array in primary macrophages (Figure 13). The mRNA expression of M1-promoting factors was comparable in macrophages from Notch1$^{+/-}$;Apoe$^{-/-}$ and Apoe$^{-/-}$ mice at basal levels. LPS/IFN-γ increased the mRNA expression of several factors involved in the M1 polarization of macrophages including macrophage migration inhibitory factor, *Il1a, Il12a, Il12b, Il15, Cxcl10, Ccl2,* and *Ccl12* in Apoe$^{-/-}$ mice and Notch1$^{+/-}$;Apoe$^{-/-}$ mice compared to basal levels (Figure 13). However, the mRNA levels of macrophage migration inhibitory factor, *tumor necrosis factor-α*, *Il12b, Il18, Ifna2*, and *Ifn-γ* were significantly lower in Notch1$^{+/-}$;Apoe$^{-/-}$ mice compared with *Apoe*$^{-/-}$ mice, suggesting differential effects of *Notch1* haploinsufficiency on macrophage polarization (Figure 13). At basal levels, significantly higher mRNA expressions of M2-differentiation–promoting factors including *Tgfβ2* (P<0.05), *Ccxl12* (P<0.0001), *Il5* (P<0.01) and *Il11* (P<0.05) were observed in the BMMs isolated from *Notch1*$^{+/-}$;*Apoe*$^{-/-}$

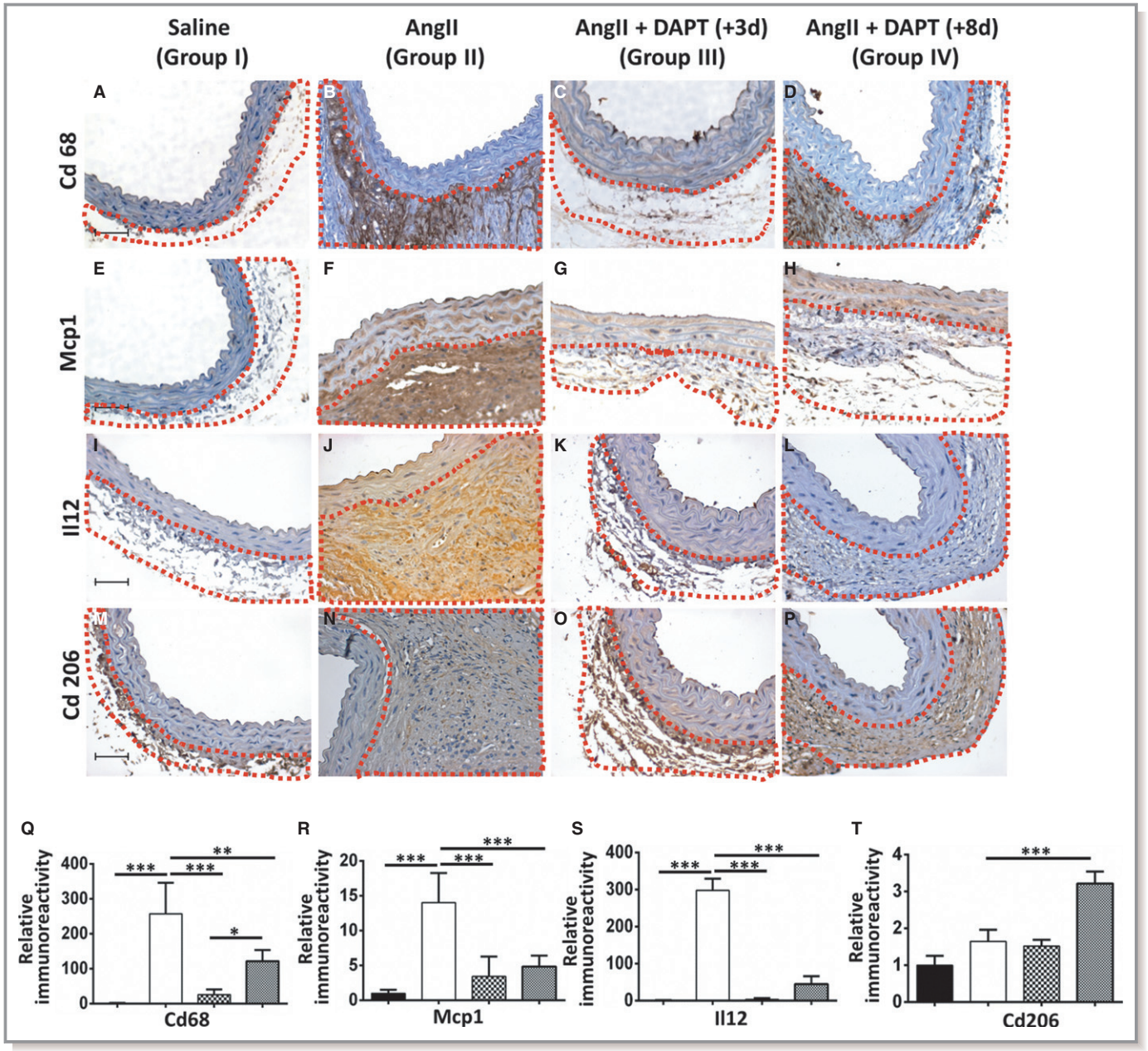

Figure 10. Notch inhibitor decreases M1-differentiated macrophages and increases M2- differentiated macrophages in the abdominal aorta of *Apoe*$^{-/-}$ mice in response to AngII. A through D Representative images of IHC showing the expression of CD68 staining as a measure of total macrophage content in *Apoe*$^{-/-}$ mice infused with saline, AngII, or DAPT at day 3 or day 8 of AngII treatment. E through H, Immunohistochemical detection of Mcp1 as a measure of inflammation in the abdominal aorta from respective experimental groups. I through P, Identification of proinflammatory M1-differentiated macrophages with antibodies against Il12 (I through L) and anti-inflammatory M2-differentiated macrophages with antibodies against Cd206 (M through P) from respective experimental groups. Dashed red lines outline the adventitial layer. Q through T, Semiquantitative analysis of CD68, Mcp1, Il12, and Cd206 IHC using Image-Pro Plus software. Six visual fields (magnification ×400) of every lesion section were randomly included to quantify the amount of immunostaining (area of staining per total area) standardized to the average area in the control group. Scale bar=50 μm. AngII indicates angiotensin II; DAPT, N-(N-[3,5-difluorophenacetyl]-L-alanyl)-S-phenylglycine t-butyl ester; IHC, immunohistochemistry.

mice compared with *Apoe*$^{-/-}$ mice (Figure 14A). In response to Il4, which promotes M2differentiation, *Notch1* haploinsufficiency demonstrated similar upregulation of this panel of cytokines (P<0.01; Figure 14B). The changes in mRNA expression of these cytokines (*Tgfβ2*, *Cxcl12*, *Il5*, and *Il11*) were confirmed with qRT-PCR using specific primers (data not shown). Interestingly, the mRNA expression of *Tgfβ2* (P<0.001) and *Il11* (P<0.001) was also significantly higher in the aortas from

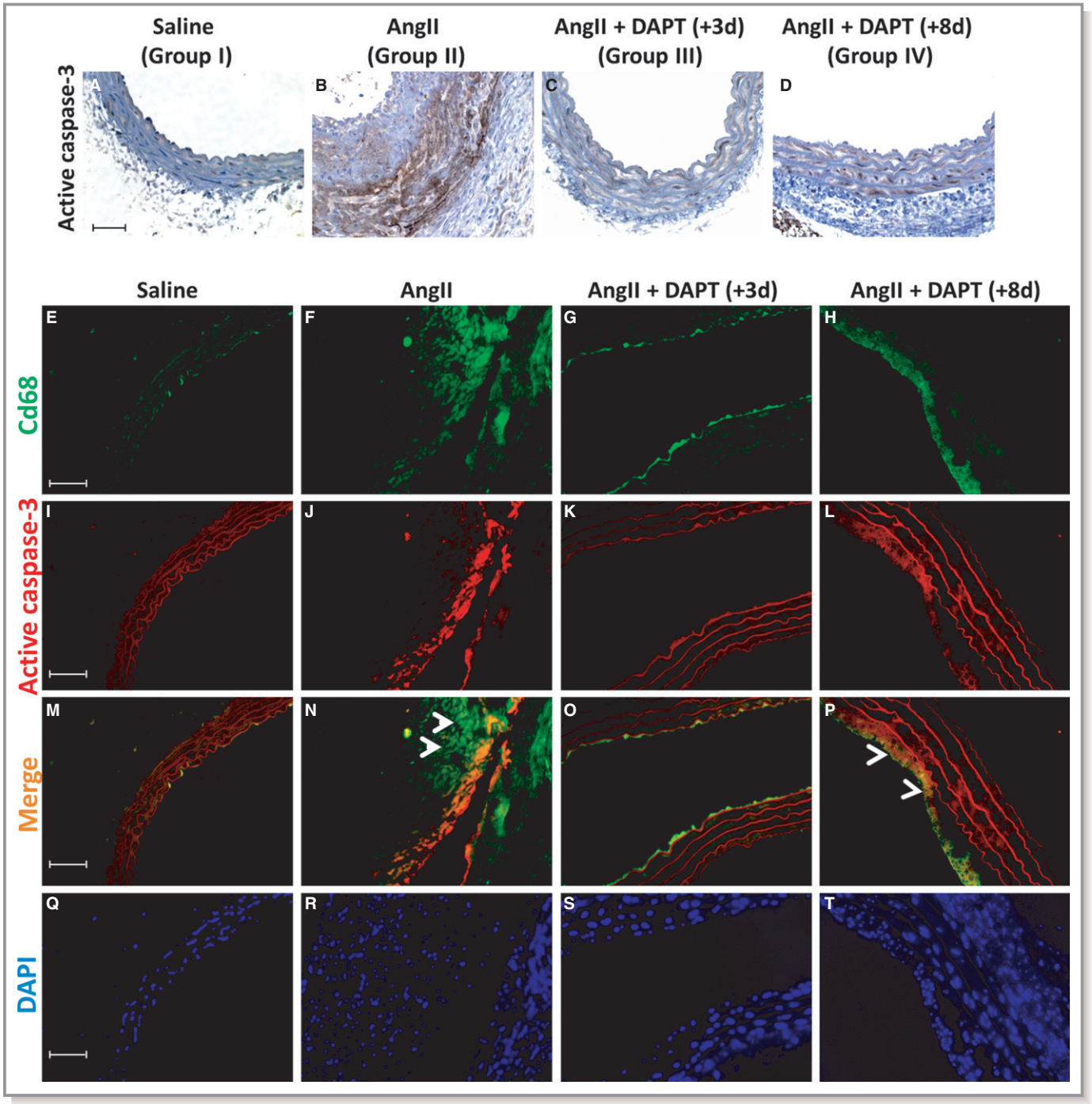

Figure 11. CD68-positive macrophages in the abdominal aorta of DAPT-treated *Apoe*$^{-/-}$ mice correlate with active caspase-3 staining. A through D, Representative images of IHC using antibodies against active caspase-3 in the adventitial region of abdominal aorta of *Apoe*$^{-/-}$ mice treated with saline, AngII, or DAPT at day 3 or day 8 of AngII infusion. E through L, Double immunofluorescence demonstrating coexpression of CD68 (green) and active caspase-3 (red) in the abdominal aorta of *Apoe*$^{-/-}$ mice treated with saline, AngII, or DAPT at day 3 or day 8 of AngII infusion. Merged images of the immunofluorescence staining are shown (M through P). Aortas from 3 mice were examined, and representative sections are shown. Scale=50 μm. All nuclei were stained by DAPI (blue; Q through T). AngII indicates angiotensin II; DAPI, 4′,6-diamidino-2-phenylindole; DAPT, N-(N-[3,5-difluorophenacetyl]-L-alanyl)-S-phenylglycine t-butyl ester; IHC, immunohistochemistry.

Notch1$^{+/-}$;*Apoe*$^{-/-}$ mice in response to AngII at day 7 compared with *Apoe*$^{-/-}$ mice (Figure 14C). These data suggested that loss of Notch1 in macrophages is associated with decreased mRNA expression of M1-phenotype–promoting factors and increased mRNA expression of M2-phenotype–promoting factors.

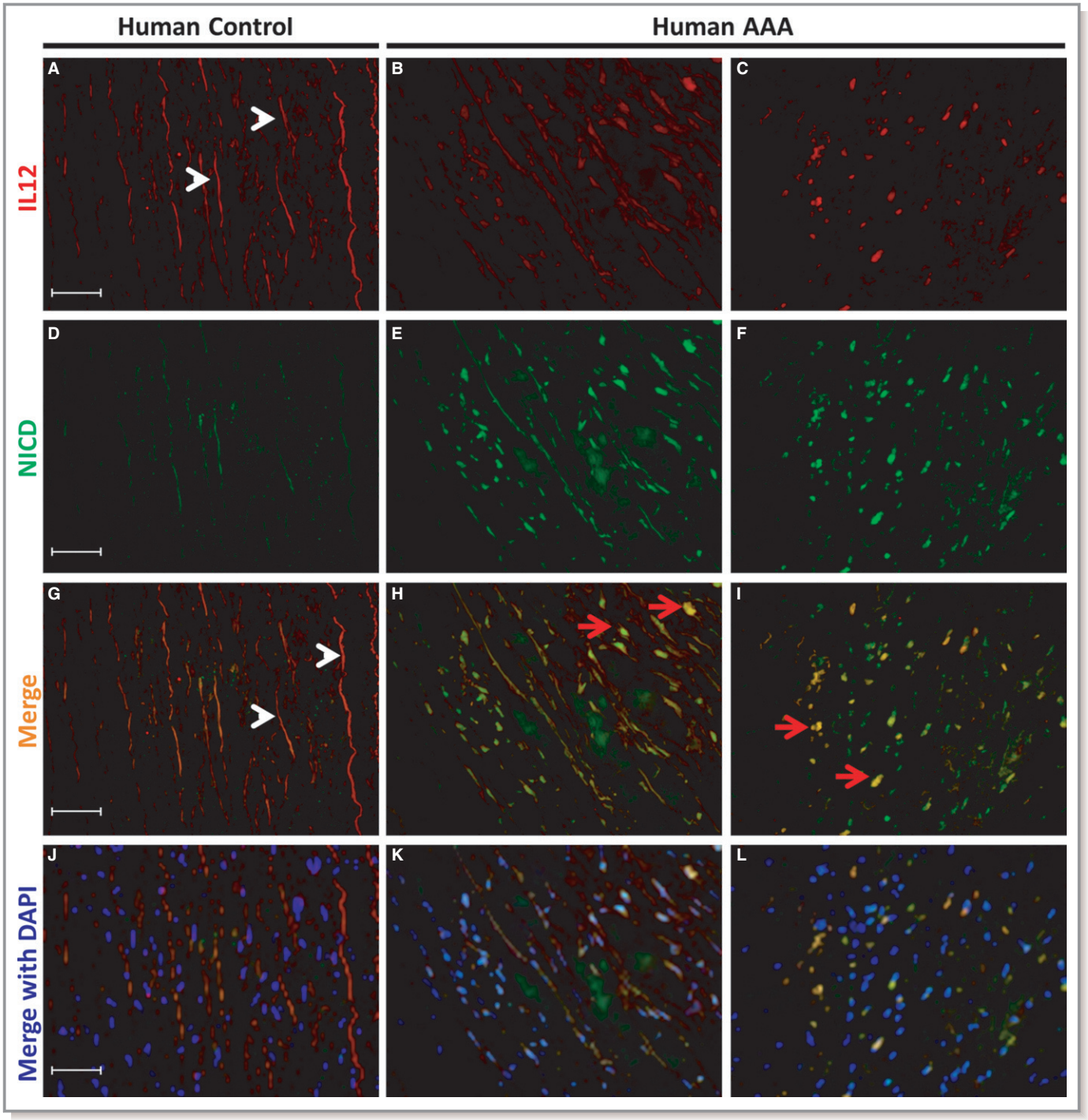

Figure 12. Increased expression of NICD localizes with the inflammatory M1 macrophages in aneurysmal aorta of human AAA. A through L, Double immunofluorescence staining for IL12 and NICD expression in the infrarenal abdominal aorta from patients with AAA (B, C, E, and F) and age-matched controls (A and D). Yellow color indicates colocalization of NICD and IL12 (red arrows in H and I). Of note, white arrowheads in A and G correspond to nonspecific autofluorescence of elastin fibrils. The arrowheads in N and P points localization of Cd68 and active caspase-3 staining. Nuclei were stained with DAPI (J through L). Scale bar=50 μm. AAA indicates abdominal aortic aneurysm; NICD, Notch1 intracellular domain.

Our in vitro data suggested crosstalk between Notch1 and Tgfβ2 signaling, which might mediate the upregulation of M2 differentiation of macrophages in the setting of AAA. We examined whether Tgfβ2 signaling was altered by DAPT in this AAA mouse model. No visible differences in the immunostaining of Tgfβ2 were observed in group 2 in response to AngII, and results were similar to saline-treated *Apoe*$^{-/-}$ mice in group 1 (Figure 14D, 14E, and 14L). Increased immunoreactivity of

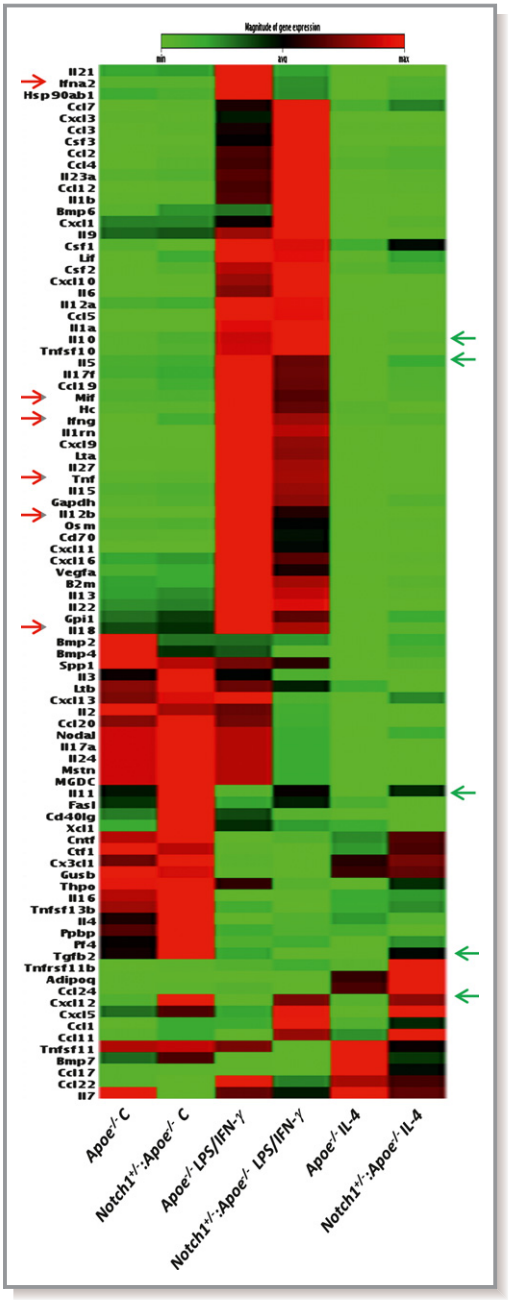

Figure 13. *Notch1* haploinsufficiency differentially affects the polarization of macrophages at basal levels and in response to stimulants. RT^2 PCR profiling array analysis of bone marrow–derived macrophages from *Apoe*$^{-/-}$ and *Notch1*$^{+/-}$; *Apoe*$^{-/-}$ mice at basal levels (C), in response to LPS/IFN-γ or IL4. Intensity of the PCR signal was standardized to housekeeping genes, as described under Methods. All values are the averages of data from 3 independent experiments. Red arrows at left point to significant change in the expression of M1-promoting genes, and green arrows at right point to the significant change in the expression of M2-promoting genes. IFN indicates interferon; IL, interleukin; LPS, lipopolysaccharide; PCR, reverse transcriptase polymerase chain reaction.

Tgfβ2 was observed in the macrophage-rich adventitial layer of abdominal aortas of DAPT-treated groups 3 and 4 compared with group 2 (Figure 14F, 14G, and 14L). The immunostaining of pSmad2, a downstream effector of Tgfβ2 signaling, was also increased in the adventitial layer of the abdominal aorta by Notch inhibitor in groups 3 and 4 compared with group 2 (Figure 14H through 14K, and 14M). In the BMMs isolated from *Apoe*$^{-/-}$ mice, recombinant Tgfβ2 increased the expression of *Arg1*, an M2-differentiation marker in the presence of IL4, whereas expression of *iNos*, an M1 differentiation marker, was decreased in the presence of LPS/IFN-γ (Figure 14N and 14O). In contrast, the Tgfβ receptor kinase inhibitor (SB-431542) decreased the expression of *Arg1* in response to IL4 while increasing the expression of *iNos* in the presence of LPS/IFN-γ, suggesting that Tgfβ2 mediates M2 activation of macrophages (Figure 14L and 14M). The data suggest that Tgfβ2 is a key player to promote the differentiation of macrophages toward the M2 phenotype and may act downstream of Notch signaling in the stabilization of AAA.

Discussion

We previously reported that *Notch1* haploinsufficiency and pharmacological inhibition protects against the formation of AAA in a mouse model by preventing the infiltration of proinflammatory macrophages at the site of vascular lesion. In this research, we studied whether Notch inhibitor is effective in stabilizing the progression of small AAA and explored the mechanism of the preventive effects of Notch inhibitor in the AngII-induced mouse model of AAA. Our study showed that treatment of small AAA with a potent pharmacological Notch inhibitor (DAPT) resulted in the reduction of progressive luminal expansion along with regeneration of tropoelastin and increased adventitial collagen content, which provides stability to the aorta. In addition, DAPT-treated mice also had decreased content of MMPs in the abdominal aorta, maintained lower *Mmp2* to *Timp3* and *Mmp9* to *Timp3* ratios and had less extracellular matrix degradation. Excessive differentiation of naïve macrophages to the M1 phenotype occurs in a mouse model of AngII-induced AAA and may contribute to pathogenesis of disease progression. *Notch1* deficiency, in contrast, is associated with upregulation of cytokines and chemokines, which promote M2 differentiation of macrophages in addition to downregulation of cytokines and chemokines, which promote M1 differentiation of macrophages. We also showed that DAPT-induced stabilization of AAA progression was associated with decreased infiltration of proinflammatory M1 macrophages and increased content of immunosuppressive M2 macrophages in the aneurysmal tissue. Finally, the data provided evidence that Notch inhibition in an AAA mouse model is associated with increased Tgfβ2 signaling, which may

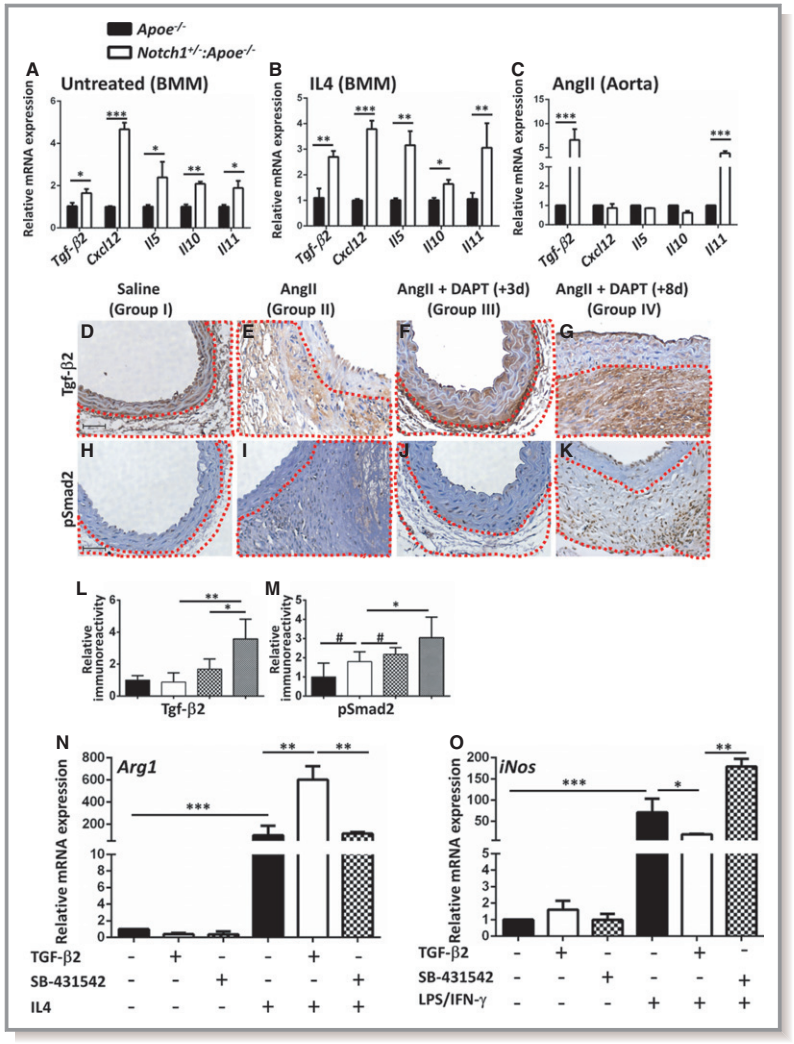

Figure 14. *Notch1* deficiency upregulates the expression of Tgfβ2 signaling in naive macrophages and in the aorta of *Apoe*$^{-/-}$ mice in response to AngII. A through C, Quantitative RT² Profiler PCR Array demonstrating expressions levels of M2-promoting genes in the BMMϕ isolated from *Apoe*$^{-/-}$ and *Notch1*$^{+/-}$;*Apoe*$^{-/-}$ mice at basal levels (untreated; A), in response to IL4 (20 ng/mL) for 48 hours (B), and in the abdominal aorta treated with AngII for 7 days (C). D through K, Representative images of IHC showing the expression Tgfβ2 (D through G) and its downstream target pSmad2 (H through K) in the abdominal aorta of *Apoe*$^{-/-}$ mice infused with saline, AngII, or DAPT at day 3 or day 8 of AngII treatment. Dashed red lines outline the adventitial layer. L and M, Semiquantitative analysis of Tgfβ2 and pSmad2 IHC using Image-Pro Plus software. Six visual fields (magnification ×400) of every lesion section were randomly included to quantify the amount of immunostaining (area of staining per total area) standardized to the average area in control group. N, qRT-PCR demonstrating the expression of *Arg1* as a measure of M2 differentiation at basal levels and in response to IL4 in BMMϕ treated with TGFβ2 (recombinant protein) or TGF-β receptor kinase inhibitor (SB-431542). O, qRT-PCR demonstrating the expression of *iNOS* as a measure of M1 differentiation at basal levels and in response to lipopolysaccharide/interferon-γ in BMMϕ treated with TGFβ2 (recombinant protein) or TGF-β receptor kinase inhibitor (SB-431542). All values are expressed as mean±SEM of 3 independent experiments. ***P<0.001; **P<0.01; *P<0.05. AngII indicates angiotensin II; BMMϕ, bone marrow derived naïve macrophages; DAPT, N-(N-[3,5-difluorophenacetyl]-L-alanyl)-S-phenylglycine t-butyl ester; IHC, immunohistochemistry; IL, interleukin; iNOS, inducible nitric oxide synthase; qRT-PCR, quantitative reverse transcriptase polymerase chain reaction; TGF, transforming growth factor.

promote M2 differentiation of naïve macrophages and initiate the repair process of abdominal aorta. These data suggest that treatment with pharmacological inhibitor of Notch signaling may be a potentially promising strategy for slowing aneurysm progression.

The elastin fragmentation and collagen degradation in the medial and adventitial layers of the aorta are expected to lead to aortic dilatation and rupture, whereas prevention of such dissolution will provide stability to the tissue.[58] Our data showed that pharmacological inhibition of Notch signaling was associated with regeneration of elastin precursors including tropoelastin and hyaluronic acid; however, it has yet to be determined if these precursors mature into elastin by crosslinking. It will also be interesting to determine whether an increase in tropoelastin in response to Notch inhibition observed in our study occurred secondarily to the reduction of the inflammatory milieu or was directly regulated by Notch signaling. The altered contents of the collagens and elastin precursors can result either from decreased synthesis or excessive breakdown.[59] Increased adventitial collagen content without substantial increase in the mRNA expression of collagen by DAPT suggests that Notch inhibitor prevents the degradation of collagens and elastins and is associated with marked improvements in the architecture of the aneurysmal tissue. Given these data, the stabilization of AAA by a Notch inhibitor might be mediated not only by inhibition of macrophage infiltration but also by regeneration of elastin and prevention of elastin and collagen degradation.

Excessive MMP activation causes dissolution of the elastin and interstitial collagenous matrix of the medial layer of aorta.[60,61] Studies have shown that MMP9 expression correlates with increasing aneurysm diameter[60,62] and MMP2 levels are elevated in the vasculature from the human aneurysm wall.[63] Consistent with other studies,[23] our data also demonstrated significant decreases in gene expression and protein content of Mmp2 and Mmp9 by Notch inhibition in the aortas of *Apoe*$^{-/-}$ mice in response to AngII. TIMPs have been found to exhibit several biochemical and physiological functions, including inhibition of pro-MMP activation and active MMPs and the induction of apoptosis. The roles of Timp1 and Timp2 in AAA seem to be controversial because targeted deletion of *Timp2* resulted in attenuation of aneurysm development, presumably through its role as a cofactor in the activation of Mmp2.[64] In contrast, the role of Timp3 remains more consistent in AAA; infusion of AngII in *Timp3*$^{-/-}$ mice led to adverse remodeling of the abdominal aorta.[65] In our studies, Notch inhibition maintained optimal ratios of Mmp2 to Timp3 and Mmp9 to Timp3, preventing degradation of the abdominal aorta by the proteolytic activity of the MMPs.

A typical response to aortic injury elicits differentiation of macrophages to a classic M1 form, which produces high levels of proinflammatory cytokines and chemokines to phagocytize apoptotic cells and damage-associated debris. However, their uncontrolled production instigates inflammation and delivers proteolytic enzymes that digest extracellular matrix and render AAA unstable and progressive, associated with high levels of Il12 and iNos production.[66] Macrophages can alternatively be programmed to an immunomodulatory M2 phenotype, which counteracts the effects of M1 macrophages and dampens the inflammatory response through low Il12 and high Tgfβ2 expression profiles.[67] M2 macrophages also promote tissue repair and healing through Tgfβ2-dependent production of collagen and elastin precursors.[68,69] Our data demonstrated that under aneurysmal conditions, the delicate balance between M1 and M2 macrophages is disrupted, leading to infiltration of proinflammatory M1 macrophages at the vascular injury site and simultaneous decrease in M2-differentiated macrophages. In contrast, Notch inhibition reverses the differentiation of macrophages by increasing Cd206-positive M2 macrophages in the aorta with concomitant decrease in the Il12-positive M1 macrophages.

The mechanism by which Notch deficiency promotes differentiation of macrophages into the M2 phenotype is not fully understood, but our data suggest activation of the Tgfβ2 signaling pathway downstream of Notch1 signaling. The critical role of Tgf-β signaling in inflammation was identified by the finding that deletion of the *Tgf-βr2* leads to a lethal inflammatory disorder that was transferable through bone marrow transplantation.[70] Studies also suggest that Tgfβ2 activity is required for protection against the development and dissection of AAA in C57BL/6 mice treated with AngII.[71] Our observations suggest that Notch1 deficiency upregulates the expression of Tgfβ2 in the differentiation of macrophages into the M2 phenotype. We also demonstrated that Notch inhibitor upregulates the Tgfβ2 signaling pathway in an AAA mouse model. Although potential interactions between Notch1 and Tgfβ2 have been posited, whether Notch1 and Tgfβ2 act independently or cooperatively remains undefined.[72] Increased expressions of Cxcl12, Il5, Il10, and Il11 also predispose macrophages to M2 differentiation and have been shown to be downstream of Tgf-β signaling.[73–75] These data suggest that Notch1 deficiency might promote M2 differentiation of macrophages via direct upregulation of Tgfβ2 expression.

Several anti-inflammatory and/or anti-MMP drugs have been shown to be modestly effective in decreasing the formation of AAA in animal models.[76] However, approaches to limit progression of small AAA have not been successful, in part, because the signaling pathways involved in the disease progression may be different from the pathways implicated in the formation of the disease, making it challenging to find the key regulators of disease progression.[76–78] Due to the close association between Notch signaling and differentiation of macrophages in AAA, it is possible that Notch inhibition may

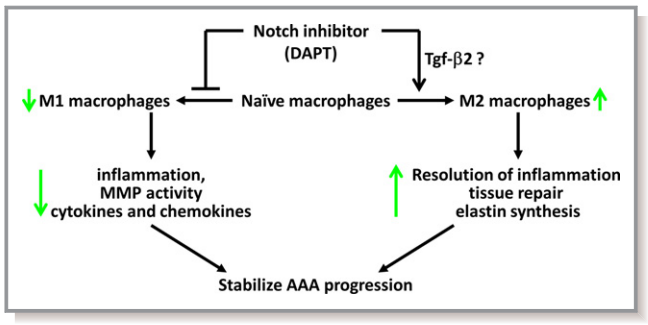

Figure 15. Schematic diagram of the proposed hypotheses of pharmacological actions of Notch inhibitor on AAA. We propose that Notch inhibitor (DAPT) decreases the overall inflammatory response by preventing M1 differentiation and modulates M2 differentiation of macrophages by Tgfβ2-dependent mechanisms to create conditions optimal to halt AAA progression. AAA indicates abdominal aortic aneurysm; DAPT, N-(N-[3,5-difluorophenacetyl]-L-alanyl)-S-phenylglycine t-butyl ester; MMP, matrix metalloproteinase; TGF, transforming growth factor.

provide stability to AAA by interfering at multiple levels in the pathways implicated in the progression of AAA (Figure 15).

Our data suggest that Notch inhibition stabilizes the progression of AAA by reducing macrophage infiltration, preventing elastin degradation, and promoting the regeneration of elastin precursors. The protective effects of Notch inhibition on AAA progression seem to be mediated by regulatory effects of Notch on macrophage differentiation. These studies also suggest that walls of established AAA still have the potential to regenerate newly synthesized elastin through pharmacological inhibition of Notch and potentially induce regression of AAA. Because drug-based therapy for AAA does not yet exist, targeting the modulation of the M2 phenotype of macrophages is an attractive approach. Identification of key molecular targets that drive M2 differentiation could lead to novel pharmacological strategies to combat other chronic inflammatory conditions.

Acknowledgments

The authors wish to thank Dave Dunaway in the Flow Cytometry Core, members of the Morphology Core at the Research Institute at Nationwide Children's Hospital for technical support, Nianyuan Huang for animal breeding, Dr Mary Cismowski for the polymerase chain reaction array experiments, Sachin Rudraraju for cell culture experiments, and Yongjie Miao for the statistical analysis of the data.

Sources of Funding

This work was supported by an American Heart Association-National Center Scientific Development Grant to Hans and funding from the Research Institute at Nationwide Children's Hospital to Hans and Garg.

Disclosures

Hans and Garg have applied for a patent related to this work.

References

1. Go AS, Mozaffarian D, Roger VL, Benjamin EJ, Berry JD, Blaha MJ, Dai S, Ford ES, Fox CS, Franco S, Fullerton HJ, Gillespie C, Hailpern SM, Heit JA, Howard VJ, Huffman MD, Judd SE, Kissela BM, Kittner SJ, Lackland DT, Lichtman JH, Lisabeth LD, Mackey RH, Magid DJ, Marcus GM, Marelli A, Matchar DB, McGuire DK, Mohler ER III, Moy CS, Mussolino ME, Neumar RW, Nichol G, Pandey DK, Paynter NP, Reeves MJ, Sorlie PD, Stein J, Towfighi A, Turan TN, Virani SS, Wong ND, Woo D, Turner MB; American Heart Association Statistics C, Stroke Statistics S. Heart disease and stroke statistics—2014 update: a report from the American Heart Association. *Circulation*. 2014;129:e28–e292.
2. Wanhainen A. How to define an abdominal aortic aneurysm—influence on epidemiology and clinical practice. *Scand J Surg*. 2008;97:105–109.
3. Moxon JV, Parr A, Emeto TI, Walker P, Norman PE, Golledge J. Diagnosis and monitoring of abdominal aortic aneurysm: current status and future prospects. *Curr Probl Cardiol*. 2010;35:512–548.
4. Filardo G, Powell JT, Martinez MA, Ballard DJ. Surgery for small asymptomatic abdominal aortic aneurysms. *Cochrane Database Syst Rev*. 2012;3:CD001835.
5. Cooper DG, King JA, Earnshaw JJ. Role of medical intervention in slowing the growth of small abdominal aortic aneurysms. *Postgrad Med J*. 2009;85:688–692.
6. Hurks R, Hoefer IE, Vink A, Pasterkamp G, Schoneveld A, Kerver M, de Vries JPPM, Tangelder MJ, Moll FL. Different effects of commonly prescribed statins on abdominal aortic aneurysm wall biology. *Eur J Vasc Endovasc Surg*. 2010;39:569–576.
7. Baxter BT, Terrin MC, Dalman RL. Medical management of small abdominal aortic aneurysms. *Circulation*. 2008;117:1883–1889.
8. Reeps C, Pelisek J, Seidl S, Schuster T, Zimmermann A, Kuehnl A, Eckstein HH. Inflammatory infiltrates and neovessels are relevant sources of MMPs in abdominal aortic aneurysm wall. *Pathobiology*. 2009;76:243–252.
9. Guo D-C, Papke CL, He R, Milewicz DM. Pathogenesis of thoracic and abdominal aortic aneurysms. *Ann N Y Acad Sci*. 2006;1085:339–352.
10. Parry DJ, Al-Barjas HS, Chappell L, Rashid ST, Ariëns RAS, Scott DJA. Markers of inflammation in men with small abdominal aortic aneurysm. *J Vasc Surg*. 2010;52:145–151.
11. Kuivaniemi H, Platsoucas CD, Tilson MD III. Aortic aneurysms: an immune disease with a strong genetic component. *Circulation*. 2008;117:242–252.
12. Blomkalns AL, Gavrila D, Thomas M, Neltner BS, Blanco VM, Benjamin SB, McCormick ML, Stoll LL, Denning GM, Collins SP, Qin Z, Daugherty A, Cassis LA, Thompson RW, Weiss RM, Lindower PD, Pinney SM, Chatterjee T, Weintraub NL. CD14 directs adventitial macrophage precursor recruitment: role in early abdominal aortic aneurysm formation. *J Am Heart Assoc*. 2013;2:e000065.
13. Wang YX, Martin-McNulty B, Freay AD, Sukovich DA, Halks-Miller M, Li WW, Vergona R, Sullivan ME, Morser J, Dole WP, Deng GG. Angiotensin II increases urokinase-type plasminogen activator expression and induces aneurysm in the abdominal aorta of apolipoprotein E-deficient mice. *Am J Pathol*. 2001;159:1455–1464.
14. Gong D, Shi W, Yi S-J, Chen H, Groffen J, Heisterkamp N. TGFbeta signaling plays a critical role in promoting alternative macrophage activation. *BMC Immunol*. 2012;13:31.
15. Monsalve E, Perez MA, Rubio A, Ruiz-Hidalgo MJ, Baladron V, Garcia-Ramirez JJ, Gomez JC, Laborda J, Diaz-Guerra MJ. Notch-1 up-regulation and signaling following macrophage activation modulates gene expression patterns known to affect antigen-presenting capacity and cytotoxic activity. *J Immunol*. 2006;176:5362–5373.
16. Gridley T. Notch signaling in vascular development and physiology. *Development*. 2007;134:2709–2718.
17. Talora C, Campese AF, Bellavia D, Felli MP, Vacca A, Gulino A, Screpanti I. Notch signaling and diseases: an evolutionary journey from a simple beginning to complex outcomes. *Biochim Biophys Acta*. 2008;1782:489–497.
18. Bray SJ. Notch signalling: a simple pathway becomes complex. *Nat Rev Mol Cell Biol*. 2006;7:678–689.
19. Gasperowicz M, Otto F. The Notch signalling pathway in the development of the mouse placenta. *Placenta*. 2008;29:651–659.
20. Foldi J, Chung AY, Xu H, Zhu J, Outtz HH, Kitajewski J, Li Y, Hu X, Ivashkiv LB. Autoamplification of Notch signaling in macrophages by TLR-induced and RBP-J–dependent induction of Jagged1. *J Immunol*. 2010;185:5023–5031.

21. Zou S, Ren P, Nguyen M, Coselli JS, Shen YH, LeMaire SA. Notch signaling in descending thoracic aortic aneurysm and dissection. *PLoS One*. 2012;7: e52833.
22. Hans CP, Koenig SN, Huang N, Cheng J, Beceiro S, Guggilam A, Kuivaniemi H, Partida-Sanchez S, Garg V. Inhibition of Notch1 signaling reduces abdominal aortic aneurysm in mice by attenuating macrophage-mediated inflammation. *Arterioscler Thromb Vasc Biol*. 2012;32:3012–3023.
23. Zheng Y-H, Li F-D, Tian C, Ren H-L, Du J, Li H-H. Notch γ-secretase inhibitor dibenzazepine attenuates angiotensin II-induced abdominal aortic aneurysm in ApoE knockout mice by multiple mechanisms. *PLoS One*. 2013;8:e83310.
24. Aoyama T, Takeshita K, Kikuchi R, Yamamoto K, Cheng XW, Liao JK, Murohara T. [gamma]-Secretase inhibitor reduces diet-induced atherosclerosis in apolipoprotein E-deficient mice. *Biochem Biophys Res Commun*. 2009; 383:216–221.
25. Hu Y-Y, Zheng M-H, Zhang R, Liang Y-M, Han H. Notch signaling pathway and cancer metastasis. In: Reichrath J, Reichrath S, eds. *Notch Signaling in Embryology and Cancer*. New York, US: Springer; 2012:186–198.
26. Osipo C, Golde TE, Osborne BA, Miele LA. Off the beaten pathway: the complex cross talk between Notch and NF-kappaB. *Lab Invest*. 2008;88:11–17.
27. Outtz HH, Tattersall IW, Kofler NM, Steinbach N, Kitajewski J. Notch1 controls macrophage recruitment and Notch signaling is activated at sites of endothelial cell anastomosis during retinal angiogenesis in mice. *Blood*. 2011;118:3436–3439.
28. Quillard T, Charreau B. Impact of Notch signaling on inflammatory responses in cardiovascular disorders. *Int J Mol Sci*. 2013;14:6863–6888.
29. Xu H, Zhu J, Smith S, Foldi J, Zhao B, Chung AY, Outtz H, Kitajewski J, Shi C, Weber S, Saftig P, Li Y, Ozato K, Blobel CP, Ivashkiv LB, Hu X. Notch-RBP-J signaling regulates the transcription factor IRF8 to promote inflammatory macrophage polarization. *Nat Immunol*. 2012;13:642–650.
30. Wang Y-C, He F, Feng F, Liu X-W, Dong G-Y, Qin H-Y, Hu X-B, Zheng M-H, Liang L, Feng L, Liang Y-M, Han H. Notch signaling determines the M1 versus M2 polarization of macrophages in antitumor immune responses. *Cancer Res*. 2010;70:4840–4849.
31. Sjolund J, Johansson M, Manna S, Norin C, Pietras A, Beckman S, Nilsson E, Ljungberg B, Axelson H. Suppression of renal cell carcinoma growth by inhibition of Notch signaling in vitro and in vivo. *J Clin Invest*. 2008;118:217–228.
32. Lillvis JH, Erdman R, Schworer CM, Golden A, Derr K, Gatalica Z, Cox LA, Shen J, Vander Heide RS, Lenk GM, Hlavaty L, Li L, Elmore JR, Franklin DP, Gray JL, Garvin RP, Carey DJ, Lancaster WD, Tromp G, Kuivaniemi H. Regional expression of HOXA4 along the aorta and its potential role in human abdominal aortic aneurysms. *BMC Physiol*. 2011;11:9.
33. Hinterseher I, Erdman R, Elmore JR, Stahl E, Pahl MC, Derr K, Golden A, Lillvis JH, Cindric MC, Jackson K, Bowen WD, Schworer CM, Chernousov MA, Franklin DP, Gray JL, Garvin RP, Gatalica Z, Carey DJ, Tromp G, Kuivaniemi H. Novel pathways in the pathobiology of human abdominal aortic aneurysms. *Pathobiology*. 2013;80:1–10.
34. Jaffe M, Sesti C, Washington IM, Du L, Dronadula N, Chin MT, Stolz DB, Davis EC, Dichek DA. Transforming growth factor-β signaling in myogenic cells regulates vascular morphogenesis, differentiation, and matrix synthesis. *Arterioscler Thromb Vasc Biol*. 2012;32:e1–e11.
35. Responte DJ, Natoli RM, Athanasiou KA. Identification of potential biophysical and molecular signalling mechanisms underlying hyaluronic acid enhancement of cartilage formation. *J R Soc Interface*. 2012;9:3564–3573.
36. Tateossian H, Morse S, Parker A, Mburu P, Warr N, Acevedo-Arozena A, Cheeseman M, Wells S, Brown SDM. Otitis media in the Tgif knockout mouse implicates TGFβ signalling in chronic middle ear inflammatory disease. *Hum Mol Genet*. 2013;22:2553–2565.
37. Burgmaier M, Liberman A, Möllmann J, Kahles F, Reith S, Lebherz C, Marx N, Lehrke M. Glucagon-like peptide-1 (GLP-1) and its split products GLP-1(9-37) and GLP-1(28-37) stabilize atherosclerotic lesions in apoe$^{-/-}$ mice. *Atherosclerosis*. 2013;231:427–435.
38. Bronkhorst IHG, Ly LV, Jordanova ES, Vrolijk J, Versluis M, Luyten GPM, Jager MJ. Detection of M2-macrophages in uveal melanoma and relation with survival. *Invest Ophthalmol Vis Sci*. 2011;52:643–650.
39. Ataka K, Asakawa A, Nagaishi K, Kaimoto K, Sawada A, Hayakawa Y, Tatezawa R, Inui A, Fujimiya M. Bone marrow-derived microglia infiltrate into the paraventricular nucleus of chronic psychological stress-loaded mice. *PLoS One*. 2013;8:e81744.
40. Bacci M, Capobianco A, Monno A, Cottone L, Di Puppo F, Camisa B, Mariani M, Brignole C, Ponzoni M, Ferrari S, Panina-Bordignon P, Manfredi AA, Rovere-Querini P. Macrophages are alternatively activated in patients with endometriosis and required for growth and vascularization of lesions in a mouse model of disease. *Am J Pathol*. 2009;175:547–556.
41. Allinen M, Beroukhim R, Cai L, Brennan C, Lahti-Domenici J, Huang H. Molecular characterization of the tumor microenvironment in breast cancer. *Cancer Cell*. 2004;6:17–32.
42. Loeys BL, Chen J, Neptune ER, Judge DP, Podowski M, Holm T, Meyers J, Leitch CC, Katsanis N, Sharifi N, Xu FL, Myers LA, Spevak PJ, Cameron DE, Backer JD, Hellemans J, Chen Y, Davis EC, Webb CL, Kress W, Coucke P, Rifkin DB, De Paepe AM, Dietz HC. A syndrome of altered cardiovascular, craniofacial, neurocognitive and skeletal development caused by mutations in TGFBR1 or TGFBR2. *Nat Genet*. 2005;37:275–281.
43. Nam D-H, Jeon H-M, Kim S, Kim MH, Lee Y-J, Lee MS, Kim H, Joo KM, Lee D-S, Price JE, Bang SI, Park W-Y. Activation of Notch signaling in a xenograft model of brain metastasis. *Clin Cancer Res*. 2008;14:4059–4066.
44. Qiu Z, Cang Y, Goff SP. c-Abl tyrosine kinase regulates cardiac growth and development. *Proc Natl Acad Sci USA*. 2010;107:1136–1141.
45. Breynaert C, Dresselaers T, Perrier C, Arijs I, Cremer J, Van Lommel L, Van Steen K, Ferrante M, Schuit F, Vermeire S, Rutgeerts P, Himmelreich U, Ceuppens JL, Geboes K, Van Assche G. Unique gene expression and MR T_2 relaxometry patterns define chronic murine dextran sodium sulphate colitis as a model for connective tissue changes in human Crohn's disease. *PLoS One*. 2013;8:e68876.
46. Oumouna-Benachour K, Hans CP, Suzuki Y, Naura A, Datta R, Belmadani S, Fallon K, Woods C, Boulares AH. Poly(ADP-ribose) polymerase inhibition reduces atherosclerotic plaque size and promotes factors of plaque stability in apolipoprotein E-deficient mice: effects on macrophage recruitment, nuclear factor-kappaB nuclear translocation, and foam cell death. *Circulation*. 2007;115:2442–2450.
47. Hans CP, Zerfaoui M, Naura AS, Catling A, Boulares AH. Differential effects of PARP inhibition on vascular cell survival and ACAT-1 expression favouring atherosclerotic plaque stability. *Cardiovasc Res*. 2008;78:429–439.
48. Bindom SM, Hans CP, Xia H, Boulares AH, Lazartigues E. Angiotensin I-converting enzyme type 2 (ACE2) gene therapy improves glycemic control in diabetic mice. *Diabetes*. 2010;59:2540–2548.
49. Hans CP, Zerfaoui M, Naura A, Troxclair D, Strong JP, Matrougui K, Boulares H. Thieno[2,3-c]isoquinolin-5-one (TIQ-A), a potent poly(ADP-ribose) polymerase inhibitor, promotes atherosclerotic plaque regression in high fat diet-fed apoe-deficient mice: effects on inflammatory markers and lipid content. *J Pharmacol Exp Ther*. 2009;329:150–158. jpet.108.145938.
50. Deckert V, Kretz B, Habbout A, Raghay K, Labbé J, Abello N, Desrumaux C, Gautier T, Lemaire-Ewing S, Maquart G, Le Guern N, Masson D, Steinmetz E, Lagrost L. Development of abdominal aortic aneurysm is decreased in mice with plasma phospholipid transfer protein deficiency. *Am J Pathol*. 2013;183:975–986.
51. Bosse K, Hans CP, Zhao N, Koenig SN, Huang N, Guggilam A, LaHaye S, Tao G, Lucchesi PA, Lincoln J, Lilly B, Garg V. Endothelial nitric oxide signaling regulates Notch1 in aortic valve disease. *J Mol Cell Cardiol*. 2013; 60:27–35.
52. Acharya A, Hans CP, Koenig SN, Nichols HA, Galindo CL, Garner HR, Merrill WH, Hinton RB, Garg V. Inhibitory role of Notch1 in calcific aortic valve disease. *PLoS One*. 2011;6:e27743.
53. Saraff K, Babamusta F, Cassis LA, Daugherty A. Aortic dissection precedes formation of aneurysms and atherosclerosis in angiotensin II-infused, apolipoprotein E-deficient mice. *Arterioscler Thromb Vasc Biol*. 2003;23:1621–1626.
54. Daugherty A, Manning M, Cassis L. Angiotensin II promotes atherosclerotic lesions and aneurysms in apolipoprotein E-deficient mice. *J Clin Invest*. 2000;105:1605–1612.
55. Golledge J, Tsao PS, Dalman RL, Norman PE. Circulating markers of abdominal aortic aneurysm presence and progression. *Circulation*. 2008;118:2382–2392.
56. Hellenthal FAMVI, Buurman WA, Wodzig WKWH, Schurink GWH. Biomarkers of AAA progression. Part 1: extracellular matrix degeneration. *Nat Rev Cardiol*. 2009;6:464–474.
57. van Es JH, van Gijn ME, Riccio O, van den Born M, Vooijs M, Begthel H, Cozijnsen M, Robine S, Winton DJ, Radtke F, Clevers H. Notch/[gamma]-secretase inhibition turns proliferative cells in intestinal crypts and adenomas into goblet cells. *Nature*. 2005;435:959–963.
58. Cho BS, Roelofs KJ, Ford JW, Henke PK, Upchurch GR Jr. Decreased collagen and increased matrix metalloproteinase-13 in experimental abdominal aortic aneurysms in males compared with females. *Surgery*. 2010;147:258–267.
59. Fischer GM. In vivo efleects of estradiol on collagen and elastin dynamics in rat aorta. *Endocrinology*. 1972;91:1227–1232.
60. Takagi H, Manabe H, Kawai N, Goto S-N, Umemoto T. Circulating matrix metalloproteinase-9 concentrations and abdominal aortic aneurysm presence: a meta-analysis. *Interact Cardiovasc Thorac Surg*. 2009;9:437–440.

61. Keeling WB, Armstrong PA, Stone PA, Bandyk DF, Shames ML. An overview of matrix metalloproteinases in the pathogenesis and treatment of abdominal aortic aneurysms. *Vasc Endovascular Surg*. 2005;39:457–464.
62. Folkesson M, Kazi M, Zhu C, Silveira A, Hemdahl A, Hamsten A, Hedin U, Swedenborg J, Eriksson P. Presence of NGAL/MMP-9 complexes in human abdominal aortic aneurysms. *Thromb Haemost*. 2007;98:427–433.
63. Koole D, Zandvoort HJA, Schoneveld A, Vink A, Vos JA, van den Hoogen LL, de Vries J-PPM, Pasterkamp G, Moll FL, van Herwaarden JA. Intraluminal abdominal aortic aneurysm thrombus is associated with disruption of wall integrity. *J Vasc Surg*. 2013;57:77–83.
64. Xiong W, Knispel R, Mactaggart J, Baxter BT. Effects of tissue inhibitor of metalloproteinase 2 deficiency on aneurysm formation. *J Vasc Surg*. 2006;44:1061–1066.
65. Basu R, Fan D, Kandalam V, Lee J, Das SK, Wang X, Baldwin TA, Oudit GY, Kassiri Z. Loss of Timp3 gene leads to abdominal aortic aneurysm formation in response to angiotensin II. *J Biol Chem*. 2012;287:44083–44096.
66. Mantovani A, Sica A, Sozzani S, Allavena P, Vecchi A, Locati M. The chemokine system in diverse forms of macrophage activation and polarization. *Trends Immunol*. 2004;25:677–686.
67. Mantovani A, Biswas SK, Galdiero MR, Sica A, Locati M. Macrophage plasticity and polarization in tissue repair and remodelling. *J Pathol*. 2013;229:176–185.
68. Cao Q, Wang Y, Zheng D, Sun Y, Wang Y, Lee VW, Zheng G, Tan TK, Ince J, Alexander SI, Harris DC. IL-10/TGF-beta-modified macrophages induce regulatory T cells and protect against adriamycin nephrosis. *J Am Soc Nephrol*. 2010;21:933–942.
69. Lopez-Castejón G, Baroja-Mazo A, Pelegrín P. Novel macrophage polarization model: from gene expression to identification of new anti-inflammatory molecules. *Cell Mol Life Sci*. 2011;68:3095–3107.
70. Levéen P, Larsson J, Ehinger M, Cilio CM, Sundler M, Sjöstrand LJ, Holmdahl R, Karlsson S. Induced disruption of the transforming growth factor beta type II receptor gene in mice causes a lethal inflammatory disorder that is transplantable. *Blood*. 2002;100:560–568.
71. Wang Y, Ait-Oufella H, Herbin O, Bonnin P, Ramkhelawon B, Taleb S, Huang J, Offenstadt G, Combadière C, Rénia L, Johnson JL, Tharaux P-L, Tedgui A, Mallat Z. TGF-β activity protects against inflammatory aortic aneurysm progression and complications in angiotensin II–infused mice. *J Clin Invest*. 2010;120:422–432.
72. Klüppel M, Wrana JL. Turning it up a Notch: cross-talk between TGFβ and Notch signaling. *Bioessays*. 2005;27:115–118.
73. Tabatabai G, Bähr O, Möhle R, Eyüpoglu IY, Boehmler AM, Wischhusen J, Rieger J, Blümcke I, Weller M, Wick W. Lessons from the bone marrow: how malignant glioma cells attract adult haematopoietic progenitor cells. *Brain*. 2005;128:2200–2211.
74. Akhtar S, Gremse F, Kiessling F, Weber C, Schober A. CXCL12 promotes the stabilization of atherosclerotic lesions mediated by smooth muscle progenitor cells in Apoe-deficient mice. *Arterioscler Thromb Vasc Biol*. 2013;33:679–686.
75. Yashiro R, Nagasawa T, Kiji M, Hormdee D, Kobayashi H, Koshy G, Nitta H, Ishikawa I. Transforming growth factor-beta stimulates interleukin-11 production by human periodontal ligament and gingival fibroblasts. *J Clin Periodontol*. 2006;33:165–171.
76. Xie X, Lu H, Moorleghen JJ, Howatt DA, Rateri DL, Cassis LA, Daugherty A. Doxycycline does not influence established abdominal aortic aneurysms in angiotensin II-infused mice. *PLoS One*. 2012;7:e46411.
77. Miyake T, Morishita R. Pharmacological treatment of abdominal aortic aneurysm. *Cardiovasc Res*. 2009;83:436–443.
78. Rughani G, Robertson L, Clarke M. Medical treatment for small abdominal aortic aneurysms. *Cochrane Database Syst Rev*. 2012;9:CD009536.